Enhanced replication of mouse adenovirus type 1 following virus-induced degradation of protein kinase R (PKR)

Running Title: MAV-1 degrades PKR during infection

Danielle E. Goodman[1,2], Carla D. Pretto[1], Tomas A. Krepostman[1], Kelly E. Carnahan[1] and Katherine R. Spindler*[1,2]

[1]Department of Microbiology and Immunology, University of Michigan, Ann Arbor, USA

[2]Cellular and Molecular Biology Program

*Corresponding author. Mailing address: Department of Microbiology and Immunology, University of Michigan Medical School, 1150 W. Medical Center Dr., 6724 Medical Science Bldg. II, Ann Arbor, MI 48109-5620

Phone (734) 615-2727

Fax: (734) 764-3562

Email: krspin@umich.edu

Total word count without references: 7251

Total word count without materials and methods or references: 5078

Abstract word count: 225

Importance word count: 144

Abstract

Protein kinase R (PKR) plays a major role in activating host immunity during infection by sensing dsRNA produced by viruses. Once activated by dsRNA, PKR phosphorylates the translation factor eIF2α, halting cellular translation. Many viruses have methods of inhibiting PKR activation or its downstream effects, circumventing protein synthesis shutdown. These include sequestering dsRNA or producing proteins that bind to and inhibit PKR activation. Here we describe our finding that in multiple cell types, PKR was depleted during mouse adenovirus type 1 (MAV-1) infection. MAV-1 did not appear to be targeting PKR at a transcriptional or translational level because total PKR mRNA levels and levels of PKR mRNA bound to polysomes were unchanged or increased during MAV-1 infection. However, inhibiting the proteasome reduced the PKR depletion seen in MAV-1-infected cells, whereas inhibiting the lysosome had no effect. This suggests that proteasomal degradation alone is responsible for PKR degradation during MAV-1 infection. Time course experiments indicate that the degradation occurs early after infection. Infecting cells with UV-inactivated virus prevented PKR degradation, whereas inhibiting viral DNA replication did not. Together these results suggest that an early viral gene is responsible. Degradation of PKR is a rare mechanism to oppose PKR activity, and it has only been described in six RNA viruses. To our knowledge, this is the first example of a DNA virus counteracting PKR by degrading it.

Importance

The first line of defense in cells during viral infection is the innate immune system, which is activated by different viral products. PKR is a part of this innate immune system and is induced by interferon and activated by dsRNA produced by DNA and RNA viruses. PKR is such

47 an important part of the antiviral response that many viral families have gene products to
48 counteract its activation or the resulting effects of its activity. Although a few RNA viruses
49 degrade PKR, this method of counteracting PKR has not been reported for any DNA viruses.
50 MAV-1 does not encode virus-associated RNAs, a human adenoviral defense against PKR
51 activation. Instead, MAV-1 degrades PKR, and it is the first DNA virus reported to do so. The
52 innate immune evasion by PKR degradation is a previously unidentified way for a DNA virus to
53 circumvent the host antiviral response.
54

55 **Introduction**

56 Activation of protein kinase R (PKR) is a major innate immune response to viral
57 infection. PKR is an interferon (IFN)-induced protein that is comprised of two major domains, an
58 N-terminal double-stranded RNA binding domain and a C-terminal serine/threonine kinase
59 domain (1, 2). PKR binds to dsRNA (3-5) and once bound, it becomes activated by dimerizing
60 and autophosphorylating (6-9). When activated, PKR phosphorylates eukaryotic translation
61 initiation factor 2α (eIF2α), causing inhibition of protein synthesis and reduced viral replication
62 (10-13). Many viruses encode gene products that block PKR activation or inhibit its ability to
63 phosphorylate eIF2α (14). A common mechanism is to produce a viral protein that binds and
64 sequesters dsRNA, blocking its interaction with PKR. Examples of this are vaccinia virus E3L
65 (15-17), influenza virus NS1 (18, 19), and Ebola virus protein VP35 (20). Other viruses produce
66 proteins or RNA that bind directly to PKR to inhibit its activation, such as herpes simplex virus
67 US11 (21, 22), HIV-1 Tat protein (23, 24) or TAR RNA (25), and human adenovirus (hAd)
68 virus-associated (VA) RNAs (10, 26-28).
69

Degradation of PKR by viruses is a less documented method of regulating PKR. To date PKR degradation has been reported in six RNA viruses: Toscana virus (TOSV) (29), Rift Valley fever virus (RVFV) (30-32), poliovirus (33, 34), foot-and-mouth disease virus (FMDV) (35, 36), encephalomyocarditis virus (EMCV, strain mengovirus) (37, 38), and enterovirus 71 (39). RVFV and TOSV both degrade PKR via proteasomal mechanisms involving a viral nonstructural protein (NSs) (32, 40, 41). RVFV NSs recruits a SCF (SKP1-CUL1-F-box)^{FBXW11} E3 ubiquitin ligase to ubiquitinate PKR and target it to the proteasome, though PKR ubiquitination could not be demonstrated (32, 41). The mechanism for PKR proteasomal degradation by NSs has not been described for TOSV (40). FMDV uses the other major cellular protein degradation pathway, the lysosome, to degrade PKR during infection (36). Though the mechanism is unclear, expression of the major FMDV protease $3C^{pro}$ is required for PKR degradation by the lysosome. However, $3C^{pro}$ does not interact with PKR, nor is its protease activity required for PKR degradation. The enterovirus A71 $3C^{pro}$ causes PKR degradation by direct interaction (39). The mechanism of PKR depletion by poliovirus is unclear, though gene expression is required, and the major poliovirus proteases (2A and 3C) are not directly involved (33). The mechanism by which mengovirus depletes PKR during infection is unknown (37, 38).

Adenoviruses are species-specific, making the study of hAd pathogenesis difficult in an animal model. MAV-1 is a useful alternative to study adenovirus pathogenesis (42-46). MAV-1 has molecular, genetic, and pathogenic similarities and differences to hAd. Their genomic structures are similar at a gross level, and both contain early genes involved in pathogenesis and immune evasion. Pathogenically, their tropisms vary, with hAd infecting epithelial cells, leading to upper respiratory and GI tract infections, and conjunctivitis, while MAV-1 infects endothelial

cells and monocytes, causing encephalitis and myocarditis. We and others have been investigating the adaptive and innate immune responses to MAV-1.

Human adenovirus VA RNAs bind PKR as a monomer, preventing its transautophosphorylation (47). However, MAV-1 does not produce VA RNAs (48), and it is not known whether MAV-1 induces PKR activation. In our studies of MAV-1 pathogenesis and the innate response, we discovered that during MAV-1 infection, PKR was depleted from cells as early as 12 hours post infection (hpi). Total PKR mRNA levels and PKR mRNA bound to polysomes were unchanged or increased during MAV-1 infection, suggesting that MAV-1 did not appear to be targeting PKR at a transcriptional or translational level. However, inhibiting the proteasome blocked the PKR depletion seen in MAV-1-infected cells, indicating that proteasomal degradation is responsible for PKR depletion during MAV-1 infection. We report results indicating that an early viral gene is likely responsible for mediating PKR degradation. To our knowledge, this is the first example of a DNA virus counteracting PKR by degrading it.

Results

Viral DNA yield is increased in PKR$^{-/-}$ mouse embryonic fibroblasts.

While PKR is an important part of the innate immune response, PKR$^{-/-}$ cells in culture are not always more susceptible to viral infection than wild type cells (49-51). PKR$^{-/-}$ mouse embryonic fibroblasts (MEFs) show increased viral yields compared to wild type MEFs when infected with vesicular stomatitis virus and influenza A (49, 50), but there is no change in viral yield during vaccinia virus infection compared to wild type cells (51). However, it was later

116 discovered that the PKR$^{-/-}$ MEF lines used are not complete PKR knockouts (52). There are two
117 categories of PKR$^{-/-}$ MEFs derived from knockout mice: N-PKR$^{-/-}$ MEFs and C-PKR$^{-/-}$ MEFs
118 (52). The PKR$^{-/-}$ MEFs derived from mice created in the Weissmann lab (53) are designated N-
119 PKR$^{-/-}$ MEFs, because the C-terminal fragment of PKR is still expressed and can be detected by
120 immunoblot when there is IFN induction (52). The fragment has the kinase catalytic activity of
121 PKR, but it does not bind dsRNA (52). The PKR$^{-/-}$ MEFs derived from mice created in the Bell
122 lab (54) are designated as C-PKR$^{-/-}$ MEFs, because the N-terminal fragment of PKR is still
123 expressed and can be detected by immunoblot with specific PKR antibodies (52). The fragment
124 is catalytically inactive, but it can still bind dsRNA (52). Susceptibility of these PKR$^{-/-}$ MEFs to
125 specific viruses may be dependent on the PKR mutation and the mechanism used by each virus
126 to circumvent PKR.
127
128 To determine whether PKR plays an important role during MAV-1 infection, we tested
129 the susceptibility of both PKR$^{-/-}$ MEF lines to MAV-1 infection. We infected wild type MEFs,
130 N-PKR$^{-/-}$ MEFs, and C-PKR$^{-/-}$ MEFs with MAV-1 at an MOI of 1 PFU/cell and collected cell
131 pellets at 48 and 72 hpi. DNA was purified from the cell pellets and analyzed for MAV-1
132 genome copies by qPCR. N-PKR$^{-/-}$ MEFs produced a significantly higher viral DNA yield than
133 wild type MEFs at 48 hpi, and both PKR mutant MEF lines had a significantly higher viral DNA
134 yield than wild type MEFs at 72 hpi (Fig. 1). Although we have not confirmed the production of
135 truncated PKR proteins in the cells in our laboratory, the results of Fig. 1 indicate that PKR
136 activation is an important antiviral response during MAV-1 infection *in vitro*.
137

Mouse PKR is depleted during MAV-1 infection.

To determine whether MAV-1 affects PKR during infection, we infected several cell types and analyzed PKR protein expression. We infected immortalized C57BL/6 MEFs, C57BL/6 primary peritoneal macrophages, and CMT93 cells (mouse rectal carcinoma cells) with MAV-1 at an MOI of 10 and collected cell lysates 24, 48, and 72 hpi. We analyzed cell lysates for the presence of PKR by immunoblot using a polyclonal antibody that detects mouse PKR. We probed blots with antibodies to actin as a loading control. To our surprise, in C57BL/6 MEFs, PKR was almost completely depleted from lysates 24 hpi and remained depleted through 72 hpi (Fig. 2A and B). PKR was also depleted compared to mock infection at 24 and 48 hpi in C57BL/6 MEFs infected at MOI 2 and 5 (Fig. S1). We also observed depletion of PKR in other cell types. In CMT93 cells, PKR was nearly undetectable at 24 hpi (Fig. 2A). In C57BL/6 primary peritoneal macrophages, PKR was decreased at 48 hpi compared to mock lysates, and absent in infected lysates at 72 hpi (Fig. 2A). This indicates that MAV-1 causes PKR depletion during infection.

To determine whether kinase activity of PKR is important for the depletion, we assayed infection of MEFs expressing a mutant form of mouse PKR with a point mutation in the kinase domain (K271R) (55). These cells, designated K271R SV40-MEFs, showed an even more rapid depletion of PKR than in WT SV40-MEFs (Fig. 2C). At 24 hpi, in K271R SV40-MEFs, 28% of PKR remained, compared to 60% in the WT SV40-MEFs. The fraction remaining at 72 hpi in K271R SV40-MEFs was 10%, compared to 30% in WT SV40-MEFs (Fig. 2C). This indicates that the PKR kinase does not have to be functional to be depleted during MAV-1 infection. Also, comparing the PKR immunoblot bands in the mock-infected WT SV40 MEFs and mutant

K271R SV40-MEFs suggests that the upper band of the PKR doublet usually seen in wild-type cells is a phospho-PKR band, because only the lower band of the PKR doublet is seen in kinase-dead mutant K271R SV40-MEFs. The data in Fig. 2A and C thus indicate that both PKR and phospho-PKR are depleted during MAV-1 infection.

MAV-1 does not cause PKR depletion by reducing steady-state levels of PKR mRNA

To determine the mechanism of PKR depletion, we first assayed whether reduction in PKR protein during MAV-1 infection was due to reduced PKR mRNA steady-state levels. We mock-infected or infected C57BL/6 MEFs and primary peritoneal macrophages at an MOI of 10 and collected cell lysates at 24, 48, and 72 hpi. We synthesized cDNA from RNA purified from these cell lysates and assayed for PKR mRNA by qPCR. In C57BL/6 MEFs, PKR mRNA levels were similar between mock and infected lysates at 24 hpi (Fig. 3A), a time point in which PKR protein levels were already greatly depleted in the infected lysates compared to mock lysates (Fig. 2). Although PKR mRNA levels were depleted 33% at 48 hpi and 40% 72 hpi in MAV-1-infected lysates compared to mock lysates, this does not correlate to the 84% and 94% reduction, respectively, in PKR protein levels at those time points (Fig. 2B). In C57BL/6 primary peritoneal macrophages, PKR mRNA levels in the infected lysates were 2-3 times higher than levels in mock lysates at all three time points assayed (Fig. 3B), even though PKR protein levels were almost completely depleted in infected lysates at 72 hpi (Fig. 2). This is evidence that MAV-1 is not causing PKR protein depletion by reducing PKR steady-state mRNA levels during infection.

184 **MAV-1 infection effects on PKR translation**

185 Because MAV-1 did not reduce PKR mRNA steady-state levels, we determined whether
186 MAV-1 causes PKR depletion by reducing translation of its mRNA. We first assayed total PKR
187 mRNA bound to ribosomes during infection. C57BL/6 MEFs were mock infected or infected at
188 an MOI of 5, and lysates were collected at 48 hpi in the presence of cycloheximide to keep the
189 mRNA bound to the ribosomes (56). Lysates were centrifuged through 25% sucrose to pellet
190 ribosomes, and RNA was purified from the pellets. The purified RNAs were used to generate
191 cDNA, which we assayed for PKR mRNA by qPCR. As a control for pelleting of ribosomes, we
192 assayed the pellets and sucrose cushion supernatants by immunoblot with antibodies to
193 ribosomal protein RPL7. We confirmed that RPL7 was only present in the pellets and not the
194 supernatants (Fig. S2). There was no significant difference between the amount of PKR mRNA
195 in the ribosome pellet of mock infected lysates compared to MAV-1-infected lysates (Fig. 4A).
196
197 To confirm the results seen in total mRNA bound to ribosomes, we also centrifuged cell
198 extracts on sucrose gradients to generate polysome profiles. This enabled us to analyze levels of
199 PKR mRNA associated with actively-translating ribosomes during infection. C57BL/6 MEFs
200 were mock infected or infected at an MOI of 2, and lysates were collected at 24 hpi in the
201 presence of cycloheximide, as above. RNA content for mock and infected lysates was estimated
202 by NanoDrop spectrophotometry, and equivalent OD amounts of RNA were centrifuged on 10-
203 50% sucrose gradients to sediment 40S and 60S ribosomal subunits, 80S ribosomes
204 (monosomes), and polyribosomes (polysomes). A typical polysome profile was obtained (Fig.
205 4B). RNA was purified from fractions containing monosomes and polysomes and then used to
206 generate cDNA, which we assayed for PKR mRNA by qPCR (Fig. 4C). As a control, GAPDH

mRNA was measured by qPCR, and PKR mRNA levels in each fraction were normalized to the GAPDH mRNA content. When the data for percentage of PKR mRNA bound to ribosomes was pooled into monosome and polysome fractions and analyzed (Fig. 4D), 90.1% and 91.8% were bound to polysomes (fractions 7-19) for mock and infected samples, respectively, compared to 9.9% and 8.2% bound to monosomes (fractions 1-6). We performed two additional polysome gradient analyses. The pooled data from all three (Fig. 4E) were similar to the data for Fig. 4D, i.e., 82.7% and 92.7% of PKR mRNA were bound to mock and infected polysomes, respectively, compared to 17.3% and 7.3% bound to monosomes. Thus, PKR protein depletion during MAV-1 infection does not appear to stem from a decrease in PKR mRNA translation.

We also assayed whether PKR mRNA might have a signal that would reduce its translation during MAV-1 infection. We constructed a plasmid that positioned sequence corresponding to the 5' UTR of PKR mRNA upstream of a reporter nanoluciferase gene (57), transfected it into C57BL/6 MEFs, then infected with MAV-1. Compared to cells transfected with a control plasmid with the human β-globin 5' UTR upstream of the reporter nanoluciferase, there was no significant difference in luciferase activity between mock infected and infected samples (Fig. S3). These data suggest that MAV-1 is not affecting PKR translation through interaction with the 5' UTR of PKR. The data are consistent with the ribosome pellet and polysome data that MAV-1 infection does not reduce PKR mRNA translation.

PKR is depleted by proteasomal degradation during MAV-1 infection.

There are two main proteolysis pathways in cells, proteasomal degradation and lysosomal degradation (58). To determine whether MAV-1 depletes PKR by either protein degradation

pathway, we first assayed whether PKR is lysosomally degraded as follows. CMT93 cells were mock infected or infected with MAV-1 and treated at the time of infection with the lysosome inhibitors ammonium chloride or chloroquine, or water (as a control). At 24 hpi, we collected lysates and analyzed them by immunoblot with antibodies to PKR. In the presence of the lysosomal degradation inhibitors, PKR was depleted by 24 hpi (Fig. 5A), indicating that lysosomal degradation was not the cause of PKR depletion during MAV-1 infection. We confirmed that the inhibitor treatment did block lysosomal degradation by incubating cells with dye-quenched bovine serum albumin (DQ BSA) in addition to the lysosomal inhibitors. DQ BSA is self-quenched until it is digested in the lysosome (59, 60), and imaging confirmed that cells treated with lysosome inhibitors did not fluoresce, but cells treated with the vehicle control (H_2O) did, as expected (Fig. 5B).

Next, we examined whether proteasomal degradation is responsible for the degradation of PKR by using proteasome inhibitors MG132 and bortezomib. These inhibit proteasome activity by binding to the active sites in the 20S subunit and blocking the proteolytic activity (61-63). We mock infected or infected C57BL/6 MEFs with MAV-1 and treated with MG132 or bortezomib in DMSO at the time of infection. At 24 hpi, we collected lysates and analyzed them by immunoblot for PKR protein levels. While PKR was depleted in the control DMSO-treated MAV-1-infected cells as expected, PKR protein was present in the MG132- and bortezomib-treated cells at levels comparable to mock infected cells (Fig. 6A and B). To rule out the possibility that PKR was present (not depleted) because the virus infection itself was inhibited by MG132 or bortezomib, we assayed viral replication of MAV-1 with MG132 and bortezomib treatment by qPCR of viral DNA. Viral replication was equivalent in all three treatment groups

253 (Fig. S4), indicating that the treatments did not affect the ability of the virus to productively
254 infect the cells. Taken together, these data indicate that MAV-1 infection results in PKR
255 depletion by causing PKR to be degraded by the proteasome during infection.
256
257 A signal for proteasomal degradation is the conjugation of ubiquitin to a protein (64, 65).
258 We examined whether PKR is ubiquitinated by immunoblot. We detected ubiquitination of a
259 positive control, mouse p53, which is degraded in the presence of MAV-1 proteins (66).
260 However, even with the use of epitope-tagged ubiquitin (67) and MG132 treatment, we were
261 unable to detect PKR ubiquitination during infection (Fig. S5). This is consistent with an
262 inability to detect PKR ubiquitination when it is degraded during RVFV infection (32). Although
263 RVFV NSs is known to recruit an E3 ligase to PKR, the authors reported that ubiquitinated PKR
264 is undetectable. Therefore, the cellular degradation signal for PKR remains unclear.
265
266 **PKR is actively depleted early in infection.**
267 We investigated when proteasomal degradation of PKR occurs. Early viral proteins are
268 expressed prior to viral DNA replication, which is then followed by late viral protein expression.
269 First, we examined the kinetics of PKR degradation to determine whether an early or late viral
270 protein was likely responsible. We mock infected and infected CMT93 cells with MAV-1 at an
271 MOI of 10 and collected lysates every six hours for 24 hours and analyzed them by immunoblot
272 with antibodies to PKR or MAV-1 early region 1A (E1A) protein, the first viral protein made
273 during infection (68). In infected cells, PKR degradation was first detected at 12 hpi (Fig. 7A),
274 and quantitation of five independent experiments showed that ~20% of the starting levels of PKR
275 protein remained at 24 hpi (Fig 7B).

In parallel, to determine the half-life of PKR in uninfected CMT93 cells, we treated CMT93 cells with cycloheximide to halt protein translation and thus production of new PKR. We collected lysates every six hours for 24 hours and analyzed by immunoblot with antibodies to PKR. After 24 hours of cycloheximide treatment, approximately 90% of the starting levels of PKR protein remained (Fig. 7A bottom, and B). Comparing the results from MAV-1 infection (Fig. 7A top, and 7B) and cycloheximide treatment of uninfected cells (Fig. 7A bottom, and 7B), we conclude that MAV-1 was actively depleting PKR protein early in infection. E1A was detected by immunoblot at 18 hpi (Fig. 7C), whereas viral DNA replication was first detected at 24 hpi in CMT93 cells (Fig. S6). Thus the 18 hpi timepoint is considered an early time point during MAV-1 infection of CMT93 cells, prior to DNA replication, suggesting the involvement of an early viral protein in PKR depletion.

An early viral function is required for PKR depletion by MAV-1

To determine whether viral gene expression or DNA replication are required for PKR degradation during infection, we infected C57BL/6 MEFs and CMT93 cells with UV-inactivated MAV-1 (which does not replicate viral DNA, Fig. S7). We infected cells at an MOI of 10 with WT MAV-1 or UV-inactivated MAV-1 and analyzed lysates from 24 and 48 hpi by immunoblot for PKR protein levels. In both cell types, while PKR was degraded by 24 hpi in the cells infected with WT MAV-1, PKR protein levels were unaffected at both time points in cells infected with UV-inactivated MAV-1 (Fig. 8A). This suggested that either gene expression or DNA replication was required for PKR degradation during MAV-1 infection.

299 We addressed whether viral DNA replication is needed for PKR degradation. We mock
300 infected or infected CMT93 cells with MAV-1 at an MOI of 10 and treated them with cytosine
301 arabinoside (araC) at the time of infection to inhibit DNA synthesis (69, 70). This would allow
302 the virus to infect the cell and produce early viral proteins, but would inhibit viral DNA
303 replication and prevent late protein synthesis. We collected lysates at 20 and 40 hpi and analyzed
304 them by immunoblot. We confirmed that araC treatment resulted in no late protein synthesis by
305 performing an immunoblot for late virion proteins (Fig. S8). In samples treated with araC, PKR
306 degradation was seen at 20 and 40 hpi (Fig. 8B), indicating that DNA replication was not
307 required for PKR degradation. Taken together, the results of Fig. 8 are consistent with early viral
308 gene expression prior to DNA replication being involved in induction of PKR degradation by
309 MAV-1.
310
311 **Discussion**
312 We have demonstrated here that PKR is antiviral in MAV-1 infections of cultured cells.
313 Surprisingly, MAV-1 infection of primary and established cultured cells depleted PKR. The
314 depletion was not due to reduced steady-state levels or reduced translation of PKR mRNA.
315 Instead, we showed that PKR depletion is inhibited by proteasome inhibitors, implicating
316 proteasomal degradation of PKR. Several lines of evidence suggest that the degradation is due to
317 a viral early function.
318
319 PKR is an IFN-inducible gene product that is an important component of the innate
320 immune response (1, 49). However, not all viruses have increased virulence in $PKR^{-/-}$ MEFs,
321 including EMCV and vaccinia virus (51, 71). While hAds produce VA RNAs that inhibit PKR

antiviral activity during infection (10, 72), MAV-1 does not produce such VA RNAs, and how MAV-1 infection is affected by PKR is first described in this report. When we infected PKR$^{-/-}$ MEFs with MAV-1, viral DNA yields were 5 to 6 times higher than viral DNA yields from wild type MEFs (Fig. 1), indicating that PKR plays an antiviral role during MAV-1 infection. At 48 hpi, the viral DNA yield from the N-MEFs was nearly 4 times higher than the C-MEFs, but by 72 hpi the viral DNA yields from both types of PKR$^{-/-}$ MEFs were similar to each other and significantly increased compared to wild type MEFs (Fig. 1). This difference in viral replication kinetics between the two types of PKR$^{-/-}$ MEFs may be due to differences in expression level and activity of the PKR fragments reportedly produced by them; we have not assayed PKR fragment production in our cells.

We examined PKR protein levels during MAV-1 infection and found that PKR was depleted from the cells as early as 12 hpi (Fig. 7). Depletion was seen in a wide variety of cell types, including immortalized C57BL/6 MEFs, primary C57BL/6 peritoneal macrophages, and CMT93 mouse colon carcinoma cells. Once depleted, PKR protein levels never returned to mock infected PKR protein levels during infection. Activation (transautophosphorylation) of PKR (6-9) was not required for this depletion, because kinase-dead mouse PKR was also depleted from K271R SV40-MEFs during infection (Fig. 2C). Both PKR and phospho-PKR were depleted in all cell types examined.

We examined several possibilities that could explain depletion of PKR protein, including PKR mRNA levels and alterations in translation. PKR mRNA levels remained unchanged during MAV-1 infection in C57BL/6 MEFs at 24 hpi and were increased in primary C57BL/6 peritoneal

345 macrophages during MAV-1 infection (Fig. 3), times when the PKR protein levels were depleted
346 (Fig. 2A). While PKR mRNAs in C57BL/6 MEFs were depleted 33% at 48 hpi and 40% at 72
347 hpi compared to mock lysates, this is not sufficient to explain the 84% and 94% reduction,
348 respectively, in PKR protein levels at those time points (Fig. 2B). More likely, the reduction in
349 PKR steady-state mRNA levels at the late infection time points can be attributed to other effects
350 from viral infection, including the degradation or inhibition of proteins that induce PKR
351 expression. For example, p53 is capable of binding to the PKR promoter and inducing its
352 expression (73), but MAV-1 proteins cause p53 proteolysis (66). Together our results in
353 C57BL/6 MEFs and macrophages suggest the virus does not cause PKR protein depletion by
354 reducing PKR steady-state mRNA levels.
355
356 The differences in total PKR mRNA levels during infection between C57BL/6 MEFs and
357 primary peritoneal macrophages (Fig. 3) is possibly due to the fact that macrophages are an
358 immune cell, while MEFs are not. PKR protein took almost 3 times as long to be completely
359 degraded during infection in macrophages compared to MEFs (72 hours versus 24 hours) (Fig.
360 2A). Total PKR mRNA levels were 2 to 3 times higher in MAV-1-infected macrophages
361 compared to mock infected macrophages, unlike the MEFs where total PKR mRNA levels were
362 unchanged or reduced 33-40% during MAV-1-infection compared to mock infected MEFs. Since
363 PKR is an IFN-stimulated gene (1, 2), higher levels of total PKR mRNA seen during infection in
364 the macrophages suggests IFN induction. This suggests that the immune response mounted by
365 the macrophages was greater than the immune response in the MEFs, and could help explain
366 why PKR took longer to degrade in macrophages compared to MEFs.
367

368 We considered whether reduced PKR levels were due to reduced PKR protein translation.
369 There was no change in the total amount of PKR mRNA bound to ribosomes during infection
370 compared to uninfected cells, nor was there a significant change in the amount of actively
371 translating PKR mRNA during infection (Fig. 4). We also found that the 5' UTR of mouse PKR
372 placed upstream of a reporter gene produced the same amount of reporter with and without
373 MAV-1 infection. These data indicate that there are not translational effects of MAV-1 infection
374 on PKR protein levels that could explain the depleted PKR levels we observed.
375
376 Inhibiting lysosomal degradation resulted in no change in PKR depletion in infected cells
377 (Fig. 5A), but adding proteasome inhibitors preserved PKR protein within cells (Fig. 6A and B).
378 This indicates that PKR is not degraded by lysosomal degradation during viral infection, but by
379 proteasomal degradation. Though PKR degradation was due to proteasome activity during
380 MAV-1 infection, we were unable to demonstrate PKR ubiquitination, although we did detect
381 ubiquitination of mouse p53 (Fig. S5). This inability to demonstrate PKR ubiquitination could be
382 explained if at any given moment there were only low levels of ubiquitinated PKR present in the
383 cell. Perhaps, increasing the time under MG132 treatment could increase the amounts of
384 ubiquitinated proteins enough so that PKR ubiquitination could be seen. However, our inability
385 to detect ubiquitinated PKR is consistent with a similar inability to identify PKR ubiquitination
386 by RVFV NSs, even though NSs is known to recruit an E3 ligase to PKR (32). Alternatively, it is
387 possible that in MAV-1 infection, PKR is degraded in a ubiquitin-independent manner, possibly
388 because of intrinsic disordered regions of PKR or binding of regulating proteins to PKR that
389 target proteins to the proteasome (74, 75).

Our experiments indicate that MAV-1 actively depletes PKR early in infection. Ongoing experiments are focused on determining the MAV-1 early protein(s) responsible for PKR degradation. Two possibilities are E4 proteins, the homologs of hAd E4orf6 and E4orf3, which we originally termed E4orfa/b and E4orfa/c, respectively (76). In human adenovirus, E4orf6 interacts with another early hAd protein, E1B 55K, to participate in an E3 ligase complex that ubiquitinates and degrades p53 via proteasomal degradation (77, 78). When MAV-1 E4orf6, E1B 55K, and mouse p53 are introduced by transfection into human cells, all three proteins interact and mouse p53 is degraded (66). If MAV-1 E4orf6 and E1B 55K form a similar complex in mouse cells, it may also degrade PKR. We have preliminary evidence that mouse p53 is ubiquitinated in C57BL/6 MEFs during MAV-1 infection, which suggests that the mouse p53 degradation seen in human cells could be paralleled by degradation of endogenous mouse p53 and mouse PKR in mouse cells, mediated by MAV-1 E4orf6 and E1B 55K during infection. Another hAd E4 protein, E4orf3, causes proteasomal degradation of transcriptional intermediary factor 1γ (79) and general transcription factor II-I (80) in a manner independent of hAd E4orf6 and E1B 55K. E4orf3 has SUMO E3 ligase and E4 elongase activity and induces sumoylation of general transcription factor II-I, leading to its proteasome-dependent degradation (80). MAV-1 E4orf3 may similarly have sumoylation activity that results ultimately in proteasome-dependent PKR degradation. Another possibility of a viral protein involved in PKR degradation is the protease encoded by MAV-1. The hAd protease is encapsidated in virions and proteolytically processes viral proteins IIIa, VI, VII, VIII, mu, and TP (81-84). However, we think it is unlikely that the MAV-1 protease degrades PKR, because we showed that UV-inactivated virus was unable to degrade PKR. We assume that UV treatment would not destroy the MAV-1 protease

412 activity, just as HSV-1 VP16 activity is not altered by UV-inactivation of HSV-1 (85), but we
413 have not tested this directly.
414
415 In summary, we demonstrated that PKR has an antiviral role during MAV-1 infection *in*
416 *vitro*, because when PKR is mutated, viral replication in MEFs is significantly higher compared
417 to wild type MEFs. Analysis of global PKR steady-state protein levels during infection showed
418 complete PKR depletion by 72 hpi in multiple cell types, including immortalized and primary
419 cells, with even faster kinetics in some. PKR transcription and translation were not decreased by
420 MAV-1 infection, whereas proteasomal inhibition prevented PKR degradation. Taken together,
421 these data suggest that MAV-1 causes PKR to be proteasomally degraded at a post-translational
422 level. This work provides new insight into possible mechanisms of adenovirus inhibition of PKR
423 by DNA viruses. PKR degradation may be induced by other adenoviruses that do not produce
424 VA RNA, which includes all animal adenoviruses except primate adenoviruses and one type of
425 fowl adenovirus (86).
426
427 **Materials and Methods**
428
429 **Cells, virus, and infections**
430 CMT93 cells (CCL-223) and C57BL/6 MEFs (SCRC-1008) were obtained from the
431 American Type Culture Collection and passaged in Dulbecco's modified eagle media (DMEM)
432 containing 5% or 10% heat-inactivated fetal bovine serum (FBS), respectively, before use.
433 Primary peritoneal macrophages were obtained from 6-10 week old C57BL/6 mice purchased
434 from Jackson Laboratory (#000664) as described (87). Briefly, 6-10 week old C57BL/6 mice

435 were injected intraperitoneally with 1.2 mL 3% thioglycolate and euthanized 3-5 days later. The
436 abdominal skin was carefully removed, exposing the peritoneum, which was then injected with 5
437 mL of sterile phosphate-buffered saline (PBS). The abdomen was massaged gently, then the PBS
438 containing the peritoneal macrophages was carefully withdrawn. The macrophages were
439 centrifuged at 100 x g for 4 minutes, red blood cells lysed in lysis buffer (0.15 M ammonium
440 chloride, 1 mM potassium bicarbonate, and 0.1 mM EDTA disodium salt) for 2 minutes at room
441 temperature, centrifuged at 100 x g for 4 minutes, washed twice in PBS, resuspended in DMEM
442 + 5% heat-inactivated FBS, and plated in 6 well plates. WT and $PKR^{-/-}$ MEFs (termed PKR WT
443 MEFs and N-$PKR^{-/-}$ MEFs, respectively, throughout this paper) were obtained from Robert
444 Silverman, Cleveland Clinic (88) and were passaged in DMEM containing 10% heat-inactivated
445 FBS before use. $PKR^{-/-}$ MEFs stably transfected with empty vector (termed C-$PKR^{-/-}$ MEFs
446 throughout this paper) were obtained from Dr. Gokhan Hotamisligil, Harvard University (89)
447 and were passaged in DMEM containing 10% heat-inactivated FBS before use. WT (SV40-
448 MEFs) and K271R PKR mutant (K271R SV40-MEFs) MEFs were obtained from Anthony
449 Sadler, Hudson Institute of Medical Research (55) and were passaged in DMEM containing 10%
450 heat-inactivated FBS before use.
451
452 Wild type mouse adenovirus type 1 (MAV-1) stock was prepared and titrated on mouse
453 NIH 3T6 fibroblasts as described previously (90). WT MAV-1 was UV-inactivated by UV-
454 treating 200 µL of virus for 10 min at 800 mJ/cm^2. UV inactivation was confirmed by qPCR and
455 plaque assay.
456

457 For infections, media was removed from cells and adsorption was performed in 0.4 mL of
458 inocula for 6-well plate 35-mm wells (unless otherwise noted) for 1 hour at 37˚C at the indicated
459 MOIs (PFU/cell). After 60 minutes, 2 mL of DMEM+5% FBS was added without removing
460 inocula; this time was designated as 0 hpi. For araC experiments, 20 µg/mL araC (Sigma C1768)
461 was added at 0 hpi and replenished every 12-16 hours.
462
463 **Immunoblots**
464 At room temperature, cells were washed once with PBS and Pierce™ RIPA lysis buffer
465 (Thermo Scientific #89900) with 1x protease inhibitors (Protease Inhibitor Cocktail Kit, Thermo
466 Scientific #78410) was added to the plate. The cells were allowed to lyse at room temperature for
467 10 minutes before being harvested and centrifuged at 4˚C at 14,000 x g for 10 minutes to remove
468 debris. Equivalent amounts of protein, determined by a BCA assay (Pierce BCA Protein Assay
469 Kit, Thermo Scientific #23227), were acetone precipitated by incubating with 4x volume ice cold
470 acetone overnight at -20˚C. Precipitated proteins were pelleted at 4˚C at 13,000 x g for 10
471 minutes and the pellets were dried for 30 minutes at room temperature. Pellets were resuspended
472 in 10 µL Pierce™ RIPA lysis buffer (Thermo Scientific #89900), 3.25 µL NuPAGE 4x LDS
473 Sample Buffer (Invitrogen Cat #NP0007), and 1.25 µL 1M DTT. Samples were incubated at
474 37˚C for 10 minutes and then loaded into a well of an 8% acrylamide gel (8.3 cm wide x 7.3 cm
475 high x 0.1 cm thick) with a 2.5% stacking gel, electrophoresed for 30 minutes at 50 V and 85
476 minutes at 150 V, and then transferred to a PVDF membrane (BioRad #1620177) for 1 hour at
477 100V at 4˚C. Blots were blocked in 5% bovine serum albumin (BSA, Sigma A7906) in tris-
478 buffered saline (BioRad #1706435) and 0.1% Tween 20 (Sigma P1379). Blots were probed with
479 primary antibodies to detect mouse PKR (Santa Cruz D-20 sc-708, 1:2000, or B-10 sc-6282,

480 1:200), mouse actin (Santa Cruz sc-1616-R, 1:1000), MAV-1 E1A (AKO-7-147, 1:1000,
481 described previously (68)), or MAV-1 late viral proteins (AKO 1-103, 1:1000, described
482 previously (91, 92)). Secondary antibodies used were IRDye 800CW anti-rabbit (Li-Cor 925-
483 32213, 1:15,000) or IgG peroxidase-conjugated anti-mouse (Jackson Immuno 515-035-062,
484 1:20,000). Blots were visualized by LI-COR Odyssey imaging (LI-COR Biosciences) or
485 enhanced chemiluminescent substrates (Pierce ECL Western Blotting Substrate #32106) and X-
486 ray film (Dot Scientific #BDB810). Densitometric quantification was performed on .tif files
487 using ImageJ software from NIH (93).
488
489 To attempt to demonstrate PKR ubiquitination status during MAV-1 infection, C57BL/6
490 MEFs were transfected with GFP- or HA-epitope tagged ubiquitin plasmids (Addgene #11928
491 and #18712, respectively) 24 hours before infection. We used Polyplus jetPRIME transfection
492 reagent (Polyplus #114-15) with 10 µg plasmid DNA and 30 µL jetPRIME reagent per 10 cm
493 plate. At 12 hpi (36 hours post transfection), we treated mock and infected C57BL/6 MEFs with
494 10 µM MG132 (Sigma M7449) for 6 hours before collecting lysates at 18 hpi in HCN buffer (50
495 mM HEPES, 150 mM NaCl, 2 mM $CaCl_2$, 1% Triton X-100 (Sigma T9284), 1x protease
496 inhibitors (Protease Inhibitor Cocktail Kit, Thermo Scientific #78410), and 5 mM N-
497 ethylmalemide). The lysates were split into two aliquots, and 3 µg PKR (D-20 sc-708,
498 discontinued) or 3 µg isotype rabbit polyclonal antibody (Jackson Immuno #011-000-002) was
499 added to lysates. After rocking samples overnight at 4˚C, 20 µL protein A agarose suspension
500 (Calbiochem/Millipore #IP02-1.5ML) was added to each and samples were rocked at 4˚C for 2
501 hours. After incubation, agarose was washed 3 times with 1 mL HCN buffer, resuspended in 40
502 µL 2x Laemmli buffer (BioRad #161-0737) with 5% 2-mercaptoethanol (Sigma M6250), and

boiled for 10 minutes. Lysate supernatants remaining after the initial PKR immunoprecipitation were then immunoprecipitated again using the same procedure but with 4 µg anti-p53 (DO-1, Santa Cruz sc-126) or 4 µg isotype mouse monoclonal antibodies (ThermoFisher Scientific #02-6200). Immunoprecipitated proteins were immunoblotted for GFP- or HA-epitope tagged ubiquitin with antibodies for GFP (1:3,000, Roche #11814460001) or HA (1:4,000, Abcam #ab9110). No ubiquitin signal was detected from the PKR immunoprecipitations, though the positive control, p53, showed ubiquitin signal with both epitope-tagged ubiquitins (data not shown). Blots were also probed for PKR (1:200, PKR B-10 sc-6282), p53 (1:200, anti-p53 sc-98), and IRDye 800CW anti-mouse (Li-Cor 925-32212, 1:15,000) to confirm the immunoprecipitations were successful, and signals for both proteins were detected (data not shown).

Viral DNA yield analysis by qPCR

Cells were washed twice with room temperature PBS and harvested by scraping into PBS, centrifuging at 100 x g for 4 minutes at 4˚C, and resuspending in PBS. Total cellular DNA was purified using the Invitrogen PureLink DNA Purification Kit (Thermo Scientific #K1820-02) and quantitated by a NanoDrop Spectrophotometer. 10 ng of total cellular DNA was analyzed by qPCR using custom primers specific to MAV-1 E1A (mE1Agenomic Fwd: 5' GCA CTC CAT GGC AGG ATT CT 3' and mE1Agenomic Rev 5' GGT CGA AGC AGA CGG TTC TTC 3') and the results were normalized to GAPDH, which was analyzed using a GAPDH-specific primer/probe set (ThermoFisher Scientific, Mm99999915_g1, #4331182).

526 **mRNA analysis by qPCR**

527 Cells were harvested by scraping into media, centrifuging at 100 x g for 4 min at 4˚C, and
528 washing the cell pellet three times with ice-cold PBS. RNA was purified using the Qiagen
529 RNeasy Mini Kit (Qiagen #74134) and stored at -80˚C. 125 ng of RNA per sample was used to
530 make cDNA using the High Capacity cDNA Reverse Transcription Kit (Applied Biosystems
531 #4368814), and 2 µL of the cDNA was analyzed by qPCR using a primer/probe set specific to
532 mouse PKR sequence (Thermo Fisher, Mm01235643_m1, #4331182). The results were
533 normalized to GAPDH, which was analyzed using a GAPDH-specific primer/probe set
534 (ThermoFisher Scientific, Mm99999915_g1, #4331182). Arbitrary units were calculated as
535 follows: Mean C_T PKR – mean C_T GAPDH = ΔC_T for sample. Arbitrary unit = 2^-ΔC_T.

536

537 **Proteasome inhibition**

538 C57BL/6 MEFs were infected at an MOI of 10, and DMSO, 1 µM MG132 (Sigma
539 M7449), or 1 µM bortezomib (Selleckchem #S1013) were added to the media after a 1 hour
540 adsorption. At 24 hpi, cells were washed once with room temperature PBS, and Pierce™ RIPA
541 lysis buffer (Thermo Scientific #89900) with 1x protease inhibitors (Protease Inhibitor Cocktail
542 Kit, Thermo Scientific #78410) was added to the plate. The cells were allowed to lyse at room
543 temperature for 10 minutes before being harvested and centrifuged at 4˚C at 14,000 x g for 10
544 minutes to remove debris.

545

546 **Lysosome inhibition and DQ BSA assay**

547 CMT93 cells were infected at an MOI of 10. After a 1 hour adsorption, 10 µL water, 10
548 mM NH_4Cl (final concentration, Baker Chemical Company #0660-1), or 60 µM chloroquine

549 (final concentration, Sigma C6628) was added to the media. At 24 hpi, at room temperature,
550 cells were washed once with PBS and Pierce™ RIPA lysis buffer (Thermo Scientific #89900)
551 with 1x protease inhibitors (Protease Inhibitor Cocktail Kit, Thermo Scientific #78410) was
552 added to the plate. The cells were allowed to lyse at room temperature for 10 minutes before
553 being harvested and centrifuged at 4˚C at 14,000 x g for 10 minutes to remove debris.
554
555 The DQ BSA assay was performed as described (60). Briefly, C57BL/6 MEFs and
556 CMT93 cells were plated at 1.5 x 10^5 cells/plate or 3 x 10^5 cells/plate, respectively, in MatTek
557 Glass Bottom Microwell Dishes (Part No: P35G-1.5-14C) with 2 mL of DMEM + 10% or 5%
558 FBS, respectively. The next day, the cell media was treated with 10 µL water, 10 mM NH_4Cl
559 (final concentration), or 60 µM chloroquine (final concentration, Sigma C6628). Four hours after
560 adding inhibitors, DQ Red BSA (Invitrogen Cat #D12051) was added to the media to a final
561 concentration of 5 µg/mL in 2 mL DMEM + 10% or 5% FBS, respectively. At 24 hours post
562 treatment, the cells were imaged on a Nikon TE300 inverted microscope equipped with a
563 mercury arc lamp, Plan-Apochromat 60x, 1.4 NA objective, cooled digital CCD camera (Quantix
564 Photometrics, Tucson, AZ), and a temperature-controlled stage, set at 37˚C. To image the DQ-
565 BSA, we used an excitation filter centered at 572 nm and an emission filter centered at 635 nm.
566 The exposure time was the same for all images.
567
568 **Ribosome pelleting**
569 Ribosomes were pelleted as described (94). Briefly, C57BL/6 MEFs were plated on 10
570 cm plates, 3x10^5 cells per plate. The next day, the cells (~90% confluent) were infected with
571 MAV-1 at an MOI of 5. C57BL/6 MEF lysates were collected at 48 hpi by scraping the cells in

572 ice-cold PBS containing 100 µg/mL cycloheximide (Sigma C7698), pelleting, and resuspending
573 in lysis buffer, which was 10 mM HEPES pH 7.5, 100 mM KCl, 5 mM $MgCl_2$, 4 mM DTT,
574 0.5% NP-40, 100 µg/mL cycloheximide, 20 U/mL RNasin (Promega # N2511), 10% sucrose,
575 and 1x protease inhibitors (Protease Inhibitor Cocktail Kit, Thermo Scientific #78410). Cells
576 were lysed by passage through a chilled 26G needle five times and cleared by centrifugation for
577 10 min at 21,000 x g at 4˚C. 400 µL of cleared lysate (10 OD_{260nm} units) was layered onto 25%
578 sucrose and centrifuged 29,500 rpm in an SW41 rotor (107,458 rcf average) for 4 hours at 4˚C.
579 After pelleting, the supernatant was removed with a micropipet and 350 µL of 4˚C Buffer RLT
580 Plus (from Qiagen RNeasy Mini Kit) was added to the pellet to collect the RNA. RNA was
581 purified immediately using the Qiagen RNeasy Mini Kit (Qiagen #74134) and stored at -80˚C
582 until analysis.
583
584 **Polyribosome Gradients**
585 C57BL/6 MEFs were plated on 10 cm plates, 2 x 10^6 cells per plate. The next day, the
586 cells were infected with MAV-1 at an MOI of 2. Following a standard protocol (95), 5 minutes
587 prior to collection, cycloheximide was added at a final concentration of 100 µg/mL and
588 incubated at 37˚C. Cells were collected at 24 hpi by scraping in ice-cold PBS containing 100
589 µg/mL cycloheximide, pelleting, and resuspending in 500 µL lysis buffer (20 mM Tris-Cl, 150
590 mM NaCl, 15 mM $MgCl_2$, 8% glycerol, 20 IU/mL SUPERase•In (ThermoFisher Scientific Cat#
591 AM2696), 80 IU/mL Murine RNAse Inhibitor (New England BioLabs Cat# M0314S), 0.1
592 mg/mL heparin (Sigma H3393-50), 0.1mg/mL cycloheximide, 1 mM DTT, 1x protease inhibitor
593 (Protease Inhibitor Cocktail Kit, Thermo Scientific #78410), 20 IU/mL Turbo DNAse
594 (ThermoFisher Scientific Cat# AM2238), and 1% Triton X-100 (Sigma T9284). Cells were lysed

595 by passaging through a chilled 26G needle ten times, vortexing for 30 seconds, and then
596 incubating on ice for 5 min. Lysates were cleared by centrifugation for 5 min at 14,000 x g at
597 4˚C. 500 µL of cleared lysate (10 OD_{260nm}) was layered onto a 10-50% sucrose gradient and
598 centrifuged at 35,000 rpm in an SW41 rotor (151,000 rcf) for 3 hours at 4˚C. After
599 centrifugation, gradients were pumped out of the top with a Brandel BR-188 Density Gradient
600 Fractionation System with a continuous reading of the $OD_{254\ nm}$. From 24-34 fractions (350-500
601 µL) were collected. RNA was purified from selected fractions immediately using the Qiagen
602 RNeasy Mini Kit (Qiagen #74134) and stored at -80˚C until analysis by RT-qPCR.
603
604 **Statistical analyses**
605 Data were analyzed with GraphPad Prism 7.0 software. For qPCR and densitometry
606 analyses, the data were analyzed by individual Mann-Whitney tests. A value of $P < 0.5$ was
607 considered significant.
608
609 **Acknowledgments**
610 We thank Robert Silverman, Gokhan Hotamisligil, and Anthony Sadler for PKR mutant
611 and wild type cells. We thank Katelyn Green, Becky Billmire, and Peter Todd for the use of and
612 assistance with the Brandel BR-188 Density Gradient Fractionation System and for providing the
613 nanoluciferase and firefly luciferase plasmids. We thank Zachary Mendel and Joel Swanson for
614 assistance with imaging the DQ BSA assay. We thank Jason Weinberg, Michael Imperiale,
615 Christiane Wobus, Billy Tsai, Andrew Mehle, Mitch Ledwith, Mike Mathews, Chuck Samuel,
616 and Britt Glaunsinger for helpful discussions. We thank Michael Imperiale and Christiane
617 Wobus for comments on the manuscript.

This work was supported by HHS/NIH/National Institute of Allergy and Infectious Diseases (NIAID), 5 R01AI091721 and 1 R01AI133935 (Katherine R. Spindler); and NIH Cellular and Molecular Biology Training Grant T32 GM007315, and Rackham Pre-Candidate and Candidate Student Research Grants (Danielle E. Goodman).

References

1. Meurs E, Chong K, Galabru J, Thomas NS, Kerr IM, Williams BR, Hovanessian AG. 1990. Molecular cloning and characterization of the human double-stranded RNA-activated protein kinase induced by interferon. Cell 62:379-90.
2. McCormack SJ, Thomis DC, Samuel CE. 1992. Mechanism of interferon action: identification of a RNA binding domain within the N-terminal region of the human RNA-dependent P1/eIF-2 alpha protein kinase. Virology 188:47-56.
3. Feng GS, Chong K, Kumar A, Williams BR. 1992. Identification of double-stranded RNA-binding domains in the interferon-induced double-stranded RNA-activated p68 kinase. Proc Natl Acad Sci USA 89:5447-51.
4. Kuhen KL, Samuel CE. 1997. Isolation of the interferon-inducible RNA-dependent protein kinase Pkr promoter and identification of a novel DNA element within the 5'-flanking region of human and mouse Pkr genes. Virology 227:119-30.
5. Patel RC, Sen GC. 1992. Identification of the double-stranded RNA-binding domain of the human interferon-inducible protein kinase. J Biol Chem 267:7671-6.
6. Dabo S, Meurs EF. 2012. dsRNA-dependent protein kinase PKR and its role in stress, signaling and HCV infection. Viruses 4:2598-635.
7. Mundschau LJ, Faller DV. 1994. Endogenous inhibitors of the dsRNA-dependent eIF-2 alpha protein kinase PKR in normal and ras-transformed cells. Biochimie 76:792-800.
8. Hovanessian AG, Galabru J. 1987. The double-stranded RNA-dependent protein kinase is also activated by heparin. Eur J Biochem 167:467-73.
9. Galabru J, Hovanessian A. 1987. Autophosphorylation of the protein kinase dependent on double-stranded RNA. J Biol Chem 262:15538-44.
10. Berk AJ. 2013. Adenoviridae: The viruses and their replication. *In* Knipe DM, Howley P (ed), Fields Virology, 6th ed, vol 2. Lippincott Williams & Wilkins, Philadelphia.
11. Wek RC. 2018. Role of eIF2alpha kinases in translational control and adaptation to cellular stress. Cold Spring Harb Perspect Biol 10.
12. Farrell PJ, Balkow K, Hunt T, Jackson RJ, Trachsel H. 1977. Phosphorylation of initiation factor elF-2 and the control of reticulocyte protein synthesis. Cell 11:187-200.
13. Tahara SM, Traugh JA, Sharp SB, Lundak TS, Safer B, Merrick WC. 1978. Effect of hemin on site-specific phosphorylation of eukaryotic initiation factor 2. Proc Natl Acad Sci USA 75:789-93.

14. Dzananovic E, McKenna SA, Patel TR. 2018. Viral proteins targeting host protein kinase R to evade an innate immune response: A mini review. Biotechnol Genet Eng Rev 34:33-59.
15. Chang HW, Jacobs BL. 1993. Identification of a conserved motif that is necessary for binding of the vaccinia virus E3L gene products to double-stranded RNA. Virology 194:537-47.
16. Rice AD, Turner PC, Embury JE, Moldawer LL, Baker HV, Moyer RW. 2011. Roles of vaccinia virus genes E3L and K3L and host genes PKR and RNase L during intratracheal infection of C57BL/6 mice. J Virol 85:550-67.
17. Carroll K, Elroy-Stein O, Moss B, Jagus R. 1993. Recombinant vaccinia virus K3L gene product prevents activation of double-stranded RNA-dependent, initiation factor 2 alpha-specific protein kinase. J Biol Chem 268:12837-42.
18. Lu Y, Wambach M, Katze MG, Krug RM. 1995. Binding of the influenza virus NS1 protein to double-stranded RNA inhibits the activation of the protein kinase that phosphorylates the elF-2 translation initiation factor. Virology 214:222-8.
19. Tan SL, Katze MG. 1998. Biochemical and genetic evidence for complex formation between the influenza A virus NS1 protein and the interferon-induced PKR protein kinase. J Interferon Cytokine Res 18:757-66.
20. Cardenas WB, Loo YM, Gale M, Jr., Hartman AL, Kimberlin CR, Martinez-Sobrido L, Saphire EO, Basler CF. 2006. Ebola virus VP35 protein binds double-stranded RNA and inhibits alpha/beta interferon production induced by RIG-I signaling. J Virol 80:5168-78.
21. Poppers J, Mulvey M, Khoo D, Mohr I. 2000. Inhibition of PKR activation by the proline-rich RNA binding domain of the herpes simplex virus type 1 Us11 protein. J Virol 74:11215-21.
22. Cassady KA, Gross M, Roizman B. 1998. The herpes simplex virus US11 protein effectively compensates for the gamma1(34.5) gene if present before activation of protein kinase R by precluding its phosphorylation and that of the alpha subunit of eukaryotic translation initiation factor 2. J Virol 72:8620-6.
23. Cai R, Carpick B, Chun RF, Jeang KT, Williams BR. 2000. HIV-I TAT inhibits PKR activity by both RNA-dependent and RNA-independent mechanisms. Arch Biochem Biophys 373:361-7.
24. McMillan NA, Chun RF, Siderovski DP, Galabru J, Toone WM, Samuel CE, Mak TW, Hovanessian AG, Jeang KT, Williams BR. 1995. HIV-1 Tat directly interacts with the interferon-induced, double-stranded RNA-dependent kinase, PKR. Virology 213:413-24.
25. Park H, Davies MV, Langland JO, Chang HW, Nam YS, Tartaglia J, Paoletti E, Jacobs BL, Kaufman RJ, Venkatesan S. 1994. TAR RNA-binding protein is an inhibitor of the interferon-induced protein kinase PKR. Proc Natl Acad Sci USA 91:4713-7.
26. Thimmappaya B, Weinberger C, Schneider RJ, Shenk T. 1982. Adenovirus VAI RNA is required for efficient translation of viral mRNAs at late times after infection. Cell 31:543-51.
27. Mathews MB, Grodzicker T. 1981. Virus-associated RNAs of naturally occurring strains and variants of group C adenoviruses. J Virol 38:849-62.
28. Reich PR, Forget BG, Weissman SM. 1966. RNA of low molecular weight in KB cells infected with adenovirus type 2. J Mol Biol 17:428-39.
29. Kalveram B, Ikegami T. 2013. Toscana virus NSs protein promotes degradation of double-stranded RNA-dependent protein kinase. J Virol 87:3710-8.

30. Habjan M, Pichlmair A, Elliott RM, Overby AK, Glatter T, Gstaiger M, Superti-Furga G, Unger H, Weber F. 2009. NSs protein of Rift Valley fever virus induces the specific degradation of the double-stranded RNA-dependent protein kinase. J Virol 83:4365-75.
31. Ikegami T, Narayanan K, Won S, Kamitani W, Peters CJ, Makino S. 2009. Rift Valley fever virus NSs protein promotes post-transcriptional downregulation of protein kinase PKR and inhibits eIF2alpha phosphorylation. PLoS Pathog 5:e1000287.
32. Mudhasani R, Tran JP, Retterer C, Kota KP, Whitehouse CA, Bavari S. 2016. Protein kinase R degradation Is essential for Rift Valley fever virus infection and is regulated by SKP1-CUL1-F-box (SCF)FBXW11-NSs E3 ligase. PLoS Pathog 12:e1005437.
33. Black TL, Barber GN, Katze MG. 1993. Degradation of the interferon-induced 68,000-M(r) protein kinase by poliovirus requires RNA. J Virol 67:791-800.
34. Black TL, Safer B, Hovanessian A, Katze MG. 1989. The cellular 68,000-Mr protein kinase is highly autophosphorylated and activated yet significantly degraded during poliovirus infection: Implications for translational regulation. J Virol 63:2244-51.
35. Li W, Zhu Z, Cao W, Yang F, Zhang X, Li D, Zhang K, Li P, Mao R, Liu X, Zheng H. 2016. Esterase D enhances type I interferon signal transduction to suppress foot-and-mouth disease virus replication. Mol Immunol 75:112-21.
36. Li C, Zhu Z, Du X, Cao W, Yang F, Zhang X, Feng H, Li D, Zhang K, Liu X, Zheng H. 2017. Foot-and-mouth disease virus induces lysosomal degradation of host protein kinase PKR by 3C proteinase to facilitate virus replication. Virology 509:222-231.
37. Rabouw HH, Langereis MA, Knaap RC, Dalebout TJ, Canton J, Sola I, Enjuanes L, Bredenbeek PJ, Kikkert M, de Groot RJ, van Kuppeveld FJ. 2016. Middle East respiratory coronavirus accessory protein 4a inhibits PKR-mediated antiviral stress responses. PLoS Pathog 12:e1005982.
38. Hovanessian AG, Galabru J, Meurs E, Buffet-Janvresse C, Svab J, Robert N. 1987. Rapid decrease in the levels of the double-stranded RNA-dependent protein kinase during virus infections. Virology 159:126-36.
39. Chang YH, Lau KS, Kuo RL, Horng JT. 2017. dsRNA binding domain of PKR is proteolytically released by enterovirus A71 to facilitate viral replication. Front Cell Infect Microbiol 7:284.
40. Kalveram B, Ikegami T. 2013. Toscana virus NSs protein promotes degradation of double-stranded RNA-dependent protein kinase. J Virol 87:3710-8.
41. Kainulainen M, Lau S, Samuel CE, Hornung V, Weber F. 2016. NSs virulence factor of Rift Valley fever virus engages the F-box proteins FBXW11 and beta-TRCP1 to degrade the antiviral protein kinase PKR. J Virol 90:6140-7.
42. Kring SC, King CS, Spindler KR. 1995. Susceptibility and signs associated with mouse adenovirus type 1 infection of adult outbred Swiss mice. J Virol 69:8084-8.
43. Spindler KR, Moore ML, Cauthen AN. 2007. Mouse adenoviruses, p 49-65, The mouse in biomedical research, 2nd ed, vol 2. Academic Press, New York, NY.
44. Blailock ZR, Rabin ER, Melnick JL. 1968. Adenovirus myocarditis in mice. An electron microscopic study. Exp Mol Pathol 9:84-96.
45. McCarthy MK, Procario MC, Twisselmann N, Wilkinson JE, Archambeau AJ, Michele DE, Day SM, Weinberg JB. 2015. Proinflammatory effects of interferon gamma in mouse adenovirus 1 myocarditis. J Virol 89:468-79.

46. Guida JD, Fejer G, Pirofski LA, Brosnan CF, Horwitz MS. 1995. Mouse adenovirus type 1 causes a fatal hemorrhagic encephalomyelitis in adult C57BL/6 but not BALB/c mice. J Virol 69:7674-81.
47. Mathews MB, Shenk T. 1991. Adenovirus virus-associated RNA and translation control. J Virol 65:5657-62.
48. Meissner JD, Hirsch GN, LaRue EA, Fulcher RA, Spindler KR. 1997. Completion of the DNA sequence of mouse adenovirus type 1: Sequence of E2B, L1, and L2 (18-51 map units). Virus Res 51:53-64.
49. Balachandran S, Roberts PC, Brown LE, Truong H, Pattnaik AK, Archer DR, Barber GN. 2000. Essential role for the dsRNA-dependent protein kinase PKR in innate immunity to viral infection. Immunity 13:129-41.
50. Stojdl DF, Abraham N, Knowles S, Marius R, Brasey A, Lichty BD, Brown EG, Sonenberg N, Bell JC. 2000. The murine double-stranded RNA-dependent protein kinase PKR is required for resistance to vesicular stomatitis virus. J Virol 74:9580-5.
51. Xiang Y, Condit RC, Vijaysri S, Jacobs B, Williams BR, Silverman RH. 2002. Blockade of interferon induction and action by the E3L double-stranded RNA binding proteins of vaccinia virus. J Virol 76:5251-9.
52. Baltzis D, Li S, Koromilas AE. 2002. Functional characterization of pkr gene products expressed in cells from mice with a targeted deletion of the N terminus or C terminus domain of PKR. J Biol Chem 277:38364-72.
53. Yang YL, Reis LF, Pavlovic J, Aguzzi A, Schafer R, Kumar A, Williams BR, Aguet M, Weissmann C. 1995. Deficient signaling in mice devoid of double-stranded RNA-dependent protein kinase. EMBO J 14:6095-106.
54. Abraham N, Stojdl DF, Duncan PI, Methot N, Ishii T, Dube M, Vanderhyden BC, Atkins HL, Gray DA, McBurney MW, Koromilas AE, Brown EG, Sonenberg N, Bell JC. 1999. Characterization of transgenic mice with targeted disruption of the catalytic domain of the double-stranded RNA-dependent protein kinase, PKR. J Biol Chem 274:5953-62.
55. Yim HC, Wang D, Yu L, White CL, Faber PW, Williams BR, Sadler AJ. 2016. The kinase activity of PKR represses inflammasome activity. Cell Res 26:367-79.
56. Felicetti L, Colombo B, Baglioni C. 1966. Inhibition of protein synthesis in reticulocytes by antibiotics. II. The site of action of cycloheximide, streptovitacin A and pactamycin. Biochim Biophys Acta 119:120-9.
57. Kearse MG, Green KM, Krans A, Rodriguez CM, Linsalata AE, Goldstrohm AC, Todd PK. 2016. CGG repeat-associated non-AUG translation utilizes a cap-dependent scanning mechanism of initiation to produce toxic proteins. Mol Cell 62:314-322.
58. Cooper GM. 2000. Protein Degradation, The Cell: A Molecular Approach, 2nd ed. Sinauer Associates, Sunderland, MA.
59. Marwaha R, Sharma M. 2017. DQ-Red BSA Trafficking Assay in Cultured Cells to Assess Cargo Delivery to Lysosomes. Bio Protoc 7.
60. Palm W, Park Y, Wright K, Pavlova NN, Tuveson DA, Thompson CB. 2015. The utilization of extracellular proteins as nutrients is suppressed by mTORC1. Cell 162:259-270.
61. Guo N, Peng Z. 2013. MG132, a proteasome inhibitor, induces apoptosis in tumor cells. Asia Pac J Clin Oncol 9:6-11.

62. Chen D, Frezza M, Schmitt S, Kanwar J, Dou QP. 2011. Bortezomib as the first proteasome inhibitor anticancer drug: current status and future perspectives. Curr Cancer Drug Targets 11:239-53.
63. Berkers CR, Verdoes M, Lichtman E, Fiebiger E, Kessler BM, Anderson KC, Ploegh HL, Ovaa H, Galardy PJ. 2005. Activity probe for in vivo profiling of the specificity of proteasome inhibitor bortezomib. Nat Methods 2:357-62.
64. Ciechanover A, Heller H, Elias S, Haas AL, Hershko A. 1980. ATP-dependent conjugation of reticulocyte proteins with the polypeptide required for protein degradation. Proc Natl Acad Sci USA 77:1365-8.
65. Hershko A, Ciechanover A, Heller H, Haas AL, Rose IA. 1980. Proposed role of ATP in protein breakdown: conjugation of protein with multiple chains of the polypeptide of ATP-dependent proteolysis. Proc Natl Acad Sci USA 77:1783-6.
66. Gilson T, Blanchette P, Ballmann MZ, Papp T, Penzes JJ, Benko M, Harrach B, Branton PE. 2016. Using the E4orf6-Based E3 ubiquitin ligase as a tool to analyze the evolution of adenoviruses. J Virol 90:7350-7367.
67. Bernardi KM, Williams JM, Inoue T, Schultz A, Tsai B. 2013. A deubiquitinase negatively regulates retro-translocation of nonubiquitinated substrates. Mol Biol Cell 24:3545-56.
68. Smith K, Ying B, Ball AO, Beard CW, Spindler KR. 1996. Interaction of mouse adenovirus type 1 early region 1A protein with cellular proteins pRb and p107. Virology 224:184-97.
69. Mayne LV. 1984. Inhibitors of DNA synthesis (aphidicolin and araC/HU) prevent the recovery of RNA synthesis after UV-irradiation. Mutat Res 131:187-91.
70. Zittoun J, Marquet J, David JC, Maniey D, Zittoun R. 1989. A study of the mechanisms of cytotoxicity of Ara-C on three human leukemic cell lines. Cancer Chemother Pharmacol 24:251-5.
71. Zhou A, Paranjape JM, Der SD, Williams BR, Silverman RH. 1999. Interferon action in triply deficient mice reveals the existence of alternative antiviral pathways. Virology 258:435-40.
72. Ma Y, Mathews MB. 1996. Structure, function, and evolution of adenovirus-associated RNA: a phylogenetic approach. J Virol 70:5083-99.
73. Yoon CH, Lee ES, Lim DS, Bae YS. 2009. PKR, a p53 target gene, plays a crucial role in the tumor-suppressor function of p53. Proc Natl Acad Sci USA 106:7852-7.
74. Baugh JM, Viktorova EG, Pilipenko EV. 2009. Proteasomes can degrade a significant proportion of cellular proteins independent of ubiquitination. J Mol Biol 386:814-27.
75. Maupin-Furlow J. 2011. Proteasomes and protein conjugation across domains of life. Nat Rev Microbiol 10:100-11.
76. Kring SC, Ball AO, Spindler KR. 1992. Transcription mapping of mouse adenovirus type 1 early region 4. Virology 190:248-55.
77. Querido E, Blanchette P, Yan Q, Kamura T, Morrison M, Boivin D, Kaelin WG, Conaway RC, Conaway JW, Branton PE. 2001. Degradation of p53 by adenovirus E4orf6 and E1B55K proteins occurs via a novel mechanism involving a Cullin-containing complex. Genes Dev 15:3104-17.
78. Harada JN, Shevchenko A, Shevchenko A, Pallas DC, Berk AJ. 2002. Analysis of the adenovirus E1B-55K-anchored proteome reveals its link to ubiquitination machinery. J Virol 76:9194-206.

837 79. Forrester NA, Patel RN, Speiseder T, Groitl P, Sedgwick GG, Shimwell NJ, Seed RI,
838 Catnaigh PO, McCabe CJ, Stewart GS, Dobner T, Grand RJ, Martin A, Turnell AS. 2012.
839 Adenovirus E4orf3 targets transcriptional intermediary factor 1gamma for proteasome-
840 dependent degradation during infection. J Virol 86:3167-79.
841 80. Sohn SY, Hearing P. 2016. The adenovirus E4-ORF3 protein functions as a SUMO E3
842 ligase for TIF-1gamma sumoylation and poly-SUMO chain elongation. Proc Natl Acad
843 Sci USA 113:6725-30.
844 81. Weber J. 1976. Genetic analysis of adenovirus type 2 III. Temperature sensitivity of
845 processing viral proteins. J Virol 17:462-71.
846 82. Anderson CW, Baum PR, Gesteland RF. 1973. Processing of adenovirus 2-induced
847 proteins. J Virol 12:241-52.
848 83. Weber JM, Anderson CW. 1988. Identification of the gene coding for the precursor of
849 adenovirus core protein X. J Virol 62:1741-5.
850 84. Anderson CW. 1990. The proteinase polypeptide of adenovirus serotype 2 virions.
851 Virology 177:259-72.
852 85. Sanfilippo CM, Chirimuuta FN, Blaho JA. 2004. Herpes simplex virus type 1 immediate-
853 early gene expression is required for the induction of apoptosis in human epithelial HEP-
854 2 cells. J Virol 78:224-39.
855 86. Anonymous. 2011. Virus Taxonomy: Ninth report of the international committee on
856 taxonomy of viruses, p 128. *In* King AMQ, Adams MJ, Carstens EB, Lefkowitz EJ (ed).
857 Elsevier.
858 87. Ashley SL, Welton AR, Harwood KM, Van Rooijen N, Spindler KR. 2009. Mouse
859 adenovirus type 1 infection of macrophages. Virology 390:307-14.
860 88. Sawicki DL, Silverman RH, Williams BR, Sawicki SG. 2003. Alphavirus minus-strand
861 synthesis and persistence in mouse embryo fibroblasts derived from mice lacking RNase
862 L and protein kinase R. J Virol 77:1801-11.
863 89. Nakamura T, Kunz RC, Zhang C, Kimura T, Yuan CL, Baccaro B, Namiki Y, Gygi SP,
864 Hotamisligil GS. 2015. A critical role for PKR complexes with TRBP in
865 Immunometabolic regulation and eIF2alpha phosphorylation in obesity. Cell Rep 11:295-
866 307.
867 90. Cauthen AN, Welton AR, Spindler KR. 2007. Construction of mouse adenovirus type 1
868 mutants. Methods Mol Med 130:41-59.
869 91. Kajon AE, Brown CC, Spindler KR. 1998. Distribution of mouse adenovirus type 1 in
870 intraperitoneally and intranasally infected adult outbred mice. J Virol 72:1219-23.
871 92. Cauthen AN, Spindler KR. 1999. Novel expression of mouse adenovirus type 1 early
872 region 3 gp11K at late times after infection. Virology 259:119-28.
873 93. Schindelin J, Rueden CT, Hiner MC, Eliceiri KW. 2015. The ImageJ ecosystem: An open
874 platform for biomedical image analysis. Mol Reprod Dev 82:518-29.
875 94. Sheets MD, Fritz B, Hartley RS, Zhang Y. 2010. Polyribosome analysis for investigating
876 mRNA translation in Xenopus oocytes, eggs and embryos. Methods 51:152-6.
877 95. Morita M, Alain T, Topisirovic I, Sonenberg N. 2013. Polysome profiling analysis. Bio-
878 protocol 3:e833.
879

880

881 **Figure Legends**

882 **Figure 1.** Viral DNA yield is increased in PKR$^{-/-}$ mouse embryonic fibroblasts. PKR WT MEFs
883 (WT), N-PKR$^{-/-}$ MEFs (N-), and C-PKR$^{-/-}$ MEFs (C-) were infected with MAV-1 at an MOI 1
884 and collected at 48 and 72 hpi. DNA was purified from cell pellets and analyzed for MAV-1
885 genome copies by qPCR. Graph is representative of three experiments, 14 biological replicates
886 per cell line per time point. Error bars are standard error of the mean (SEM). *$P \leq 0.05$, ***$P \leq$
887 0.0002, ****$P \leq 0.0001$.

888

889 **Figure 2.** Mouse PKR is depleted during MAV-1 infection. (A) Cells (indicated at left) were
890 infected with MAV-1 (MAV) at an MOI of 10 or mock infected (mock). Cell lysates were
891 collected at the indicated times and analyzed by immunoblot with antibodies for PKR (B-10 for
892 C57BL/6 MEFs and D-20 for C57BL/6 primary peritoneal macrophages and CMT93 cells) and
893 actin. Blots are representative of a minimum of three independent experiments per cell line. (B)
894 Densitometry quantitation of five C57BL/6 MEFs immunoblots from A. Error bars are SEM.
895 N=5 for 24 hpi, n=4 for 48 hpi, and n=2 for 72 hpi. **$P \leq 0.01$. (C) SV40-MEFs or kinase-dead
896 (K271R) SV40-MEFs were infected with MAV-1 at an MOI of 10. Cell lysates were
897 immunoblotted as in A with PKR D-20. Numbers below are the proportion of PKR protein for
898 each time point, normalized to actin and the mock PKR protein levels from the corresponding
899 time point.

900

901 **Figure 3.** MAV-1 does not cause PKR depletion by reducing steady state levels of PKR mRNA
902 at times when the protein levels are already reduced. MEFs (A) or isolated primary peritoneal
903 macrophages (B) were harvested and infected with MAV-1 at an MOI of 10 or mock infected.

904 The cell pellets were collected and RNA was isolated. cDNA was generated from the RNA, and
905 qPCR was used to quantitate PKR mRNA levels. Each graph contains 5-7 replicates for each
906 time point from three pooled experiments. Error bars show the SEM. *$P \leq 0.05$ and **$P \leq 0.01$.
907
908 **Figure 4.** MAV-1 infection does not affect PKR translation. (A) C57BL/6 MEFs were infected
909 with MAV-1 (MAV) at an MOI of 5 or mock infected (mock) and collected at 48 hpi. Cells were
910 lysed, and cleared lysates from three 10 cm plates were layered onto 25% sucrose and
911 centrifuged to pellet ribosomes. RNA was purified from the pellets, cDNA was generated from
912 the RNA, and qPCR was used to quantitate the PKR mRNA levels. The graph contains 9
913 replicates for each time point, pooled from 3 independent experiments. Error bars show the
914 SEM. (B) C57BL/6 MEFs were infected with MAV-1 (MAV) at an MOI of 2 or mock infected
915 (mock). Cells were collected at 25 hpi and lysed; cleared lysates were layered onto 10-50%
916 sucrose gradients and centrifuged. Gradients were collected from the top and pumped through a
917 UV spectrophotometer, and 34 fractions were collected. The gradients are displayed with the
918 bottom fractions to the right. The UV trace of the first 10 fractions (including 40S and 60S
919 ribosomal subunits) is not shown. (C) RNA was purified from each fraction of the gradients in B.
920 cDNA was generated from the RNA, and qPCR was used to quantitate PKR mRNA in each
921 fraction and displayed as the percent of total PKR mRNA associated with ribosomes. B and C
922 are results from one representative experiment of 3 independent experiments. (D) Percentage of
923 total PKR mRNA associated with monosomes (fractions 1-6) and polysomes (fractions 7-19)
924 from the trial displayed in B and C were pooled for mock and infected samples. The percentages
925 represented by each bar are displayed below each bar. (E) Pooled monosome and polysome data
926 as described in D from three independent experiments. Error bars show the SEM. The

927 percentages represented by each bar are displayed below each bar. There were no significant
928 differences between mock and infected samples (A, E).
929
930 **Figure 5.** PKR is not depleted by lysosomal degradation during MAV-1 infection. (A) CMT93
931 cells were infected with MAV-1 (MAV) at an MOI of 10 or mock infected (mock) and treated
932 with 10 mM ammonium chloride or 60 μM chloroquine to inhibit lysosomal degradation, or
933 water, as a control. Cell lysates were analyzed by immunoblot with antibodies for PKR (D-20)
934 and actin. Blots are representative of three independent experiments. (B) Inhibitors were tested
935 for activity using a DQ BSA assay; the DQ BSA molecule will only fluoresce if lysosomal
936 degradation is functional. Uninfected cells were treated as indicated and imaged by fluorescence
937 microscopy.
938
939 **Figure 6.** PKR is depleted by proteasomal degradation during MAV-1 infection. (A) C57BL/6
940 MEFs were infected with MAV-1 (MAV) at an MOI of 10 or mock infected (mock) and treated
941 with DMSO (vehicle for inhibitors), 1 μM MG132, or 1 μM bortezomib. Cell lysates were were
942 analyzed by immunoblot with antibodies for PKR (D-20) and actin. Blots are representative of
943 four independent experiments. (B) Densitometry quantitation of four independent experiments.
944 Treatment with bortezomib significantly inhibited PKR depletion in MAV-1 infected cells, $*P \leq$
945 0.05.
946
947 **Figure 7.** PKR is actively depleted early in infection. (A) CMT93 cells were infected with
948 MAV-1 (MAV) at an MOI of 10 or mock infected (mock) (top), or uninfected cells were treated
949 with 50 μg/mL cycloheximide (CHX, bottom) to inhibit elongation of protein synthesis. Cell

lysates were analyzed by immunoblot with antibodies for PKR (D-20) and actin. Blots are representative of five independent experiments. (B) Densitometry quantitation of five independent experiments, $^{**}P \leq 0.01$. (C) CMT93 cell lysates from A were analyzed with a second immunoblot with antibodies for E1A and actin. Blots are representative of four replicates from two independent experiments. The E1A blot image was uniformly adjusted to a brightness of 30 and a contrast of 5 in Adobe Photoshop.

Figure 8. Early gene expression is required for PKR depletion by MAV-1. (A) Cells (as indicated at left) were infected with WT MAV-1 (WT MAV) or UV-inactivated MAV-1 (UV MAV) at an MOI of 10, or mock infected (mock). Cell lysates were analyzed by immunoblot with antibodies for PKR (D-20) and actin. Two independent wells were infected for each condition at both time points. (B) CMT93 cells were infected with WT MAV-1 (MAV) at an MOI of 10 or mock infected (mock). Infected cells were also treated (+) or not (-) with 20 µg/mL cytosine arabinasine (AraC), an inhibitor of DNA synthesis. Cell lysates were analyzed with antibodies for PKR and actin.

967 **Supplemental Figure Legends**

968 **Supplemental Figure 1.** PKR is depleted at MOIs of 2, 5, and 10. C57BL/6 MEFs were infected
969 with MAV-1 at an MOI of 2, 5, or 10 (2, 5, 10) or mock infected (mock). Cell lysates were
970 analyzed by immunoblot with antibodies for PKR (B-10) and actin. Densitometry quantitation
971 using ImageJ is listed below each lane; for each time point, the infected samples were
972 normalized to the mock. The PKR blot image was uniformly adjusted to a brightness of 150 in
973 Adobe Photoshop.

974

975 **Supplemental Figure 2.** Ribosome pelleting. To confirm that most ribosomes ended up in the
976 pellet after centrifugation through sucrose (Fig. 4A), a sample of the pellet and the corresponding
977 supernatant were analyzed by immunoblot with antibodies for RPL7 (ribosomal protein L7,
978 Abcam, 1:2000, ab72550).

979

980 **Supplemental Figure 3.** PKR mRNA 5' UTR does not result in altered reporter protein levels
981 upon MAV-1 infection. (A) C57BL/6 MEFs or (B) CMT93 cells were co-transfected with
982 pmPKR5UTRfullNL or AUG-NL-3xFLAG and pGL4.13 using jetPRIME reagents (Polyplus
983 #114-15) using the standard Polyplus protocol, with 200 ng total of plasmid and 300 µL of
984 jetPRIME reagent per 35 mm well. At 24 hours after transfection, the cells were infected with
985 MAV-1 at an MOI of 10. At 24 hpi, cells were lysed in 70 µL/well Glo Lysis Buffer (Promega
986 Corp.). After lysing, 25 µL of each lysed sample and 25 µL of OneGlo or NanoGlo (Promega
987 Corp.) was added to two wells in a black 96-well plate (Fisher Scientific #07-000-634). After 5
988 minutes, the plate was read on a Promega GloMax luminometer. Relative light units from the

pmPKR5UTRfullNL plasmid were normalized to the firefly luciferase and positive control plasmids. Graphs are representative of 7-9 biological replicates per treatment group.

Supplemental Figure 4. MG132 and bortezomib treatment do not affect MAV-1 replication at 24 hpi. C57BL/6 MEFs were infected with MAV-1 at an MOI of 10 and treated with DMSO (vehicle for inhibitors), 1 μM MG132 or bortezomib, and collected at 24 hpi. DNA was purified from cell pellets and analyzed for MAV-1 genome copies by qPCR. Graph is representative of five biological replicates per treatment group. Error bars are standard error of the mean (SEM). $*P \leq 0.05$.

Supplemental Figure 5. PKR is not detectably ubiquitinated during MAV-1 infection. CMT93 cells were transfected with a GFP-ubiquitin plasmid using standard Polyplus transfection protocols. At 24 hpt, the cells were infected with MAV-1 (MAV) at an MOI of 5 or mock infected (mock) and treated with 10 μM MG132 at 6 hpi. Cell lysates were collected at 12 hpi and immunoprecipitated with (A) PKR (D-20) or an isotype control antibody or (B) p53 (DO-1) or an isotype control antibody. Immunoprecipitated samples were analyzed by immunoblot with GFP, ubiquitin, isotype, PKR (B-10), or p53 (1801) antibodies. Input lane (mock input) contains 0.008 volume of mock infected lysate (relative to volume in immunoprecipitations). For (B) GFP and p53 were probed on separate duplicate blots.

Supplemental Figure 6. Viral DNA replication can be detected at 24 hpi by qPCR. CMT93 cells were infected with MAV-1 (MAV) at an MOI of 10 and collected every 6 hours for 24 hours. DNA was purified from cell pellets and analyzed for MAV-1 genome copies by qPCR.

Graph is representative of four to five biological replicates per treatment group. Error bars are standard error of the mean (SEM).

Supplemental Figure 7. UV-inactivated virus does not replicate viral DNA. (A) C57BL/6 MEFs or (B) CMT93 cells were infected with WT MAV-1 (WT) or UV-inactivated MAV-1 (UV) at an MOI of 10 and collected at indicated times. DNA was purified from cell pellets and analyzed for MAV-1 genome copies by qPCR. Graphs are representative of three to four biological replicates per treatment group. Error bars are standard error of the mean (SEM).

Supplemental Figure 8. AraC treatment inhibited late protein expression. CMT93 cells were infected with WT MAV-1 (MAV) at an MOI of 10 or mock infected (mock). Infected cells were also treated (+) or not (-) with 20 µg/mL cytosine arabinasine (araC), an inhibitor of DNA synthesis. Cell lysates were analyzed with antibodies for late virion proteins (AKO1-103, 1:1000). Arrowheads indicate late viral proteins.

Figure 1.

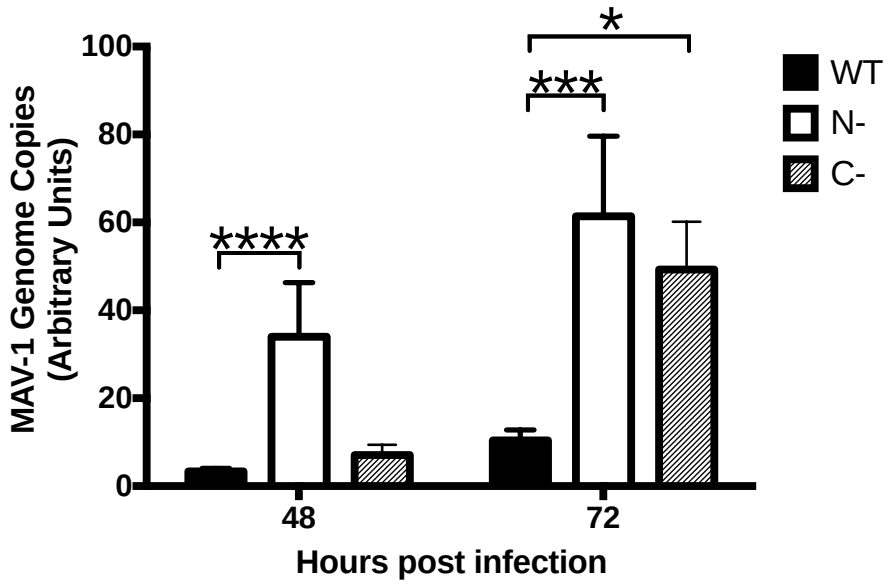

Figure 1. Viral DNA yield is increased in PKR$^{-/-}$ mouse embryonic fibroblasts. PKR WT MEFs (WT), N-PKR$^{-/-}$ MEFs (N-), and C-PKR$^{-/-}$ MEFs (C-) were infected with MAV-1 at an MOI 1 and collected at 48 and 72 hpi. DNA was purified from cell pellets and analyzed for MAV-1 genome copies by qPCR. Graph is representative of three experiments, 14 biological replicates per cell line per time point. Error bars are standard error of the mean (SEM). *$P \leq 0.05$, ***$P \leq 0.0002$, ****$P \leq 0.0001$

Figure 2.

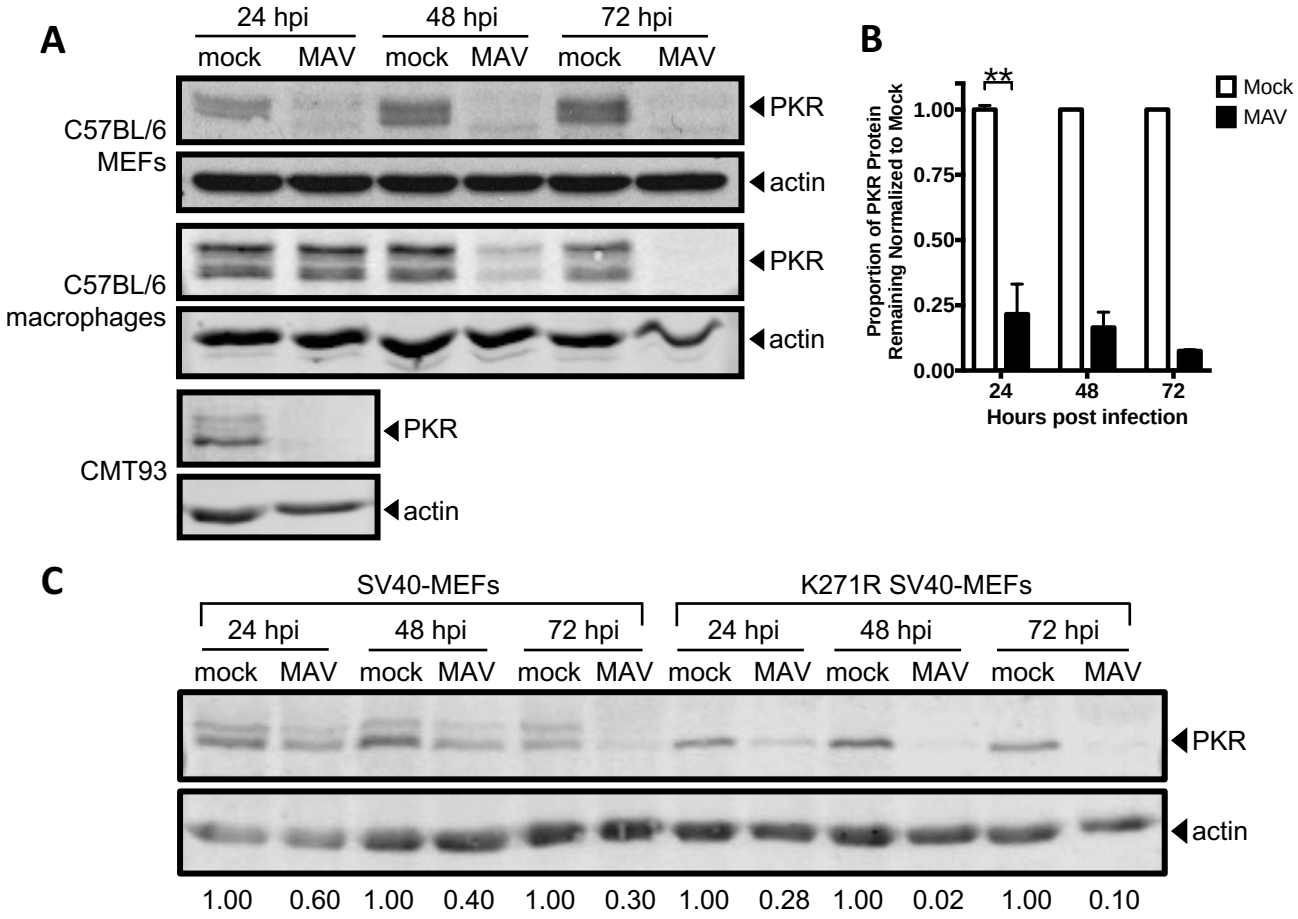

Figure 2. Mouse PKR is depleted during MAV-1 infection. (A) Cells (indicated at left) were infected with MAV-1 (MAV) at an MOI of 10 or mock infected (mock). Cell lysates were collected at the indicated times and analyzed by immunoblot with antibodies for PKR (B-10 for C57BL/6 MEFs and D-20 for C57BL/6 primary peritoneal macrophages and CMT93 cells) and actin. Blots are representative of a minimum of three independent experiments per cell line. (B) Densitometry quantitation of five C57BL/6 MEFs immunoblots from A. Error bars are SEM. N=5 for 24 hpi, n=4 for 48 hpi, and n=2 for 72 hpi. $^{**}P \leq 0.01$. (C) SV40-MEFs or kinase-dead (K271R) SV40-MEFs were infected with MAV-1 at an MOI of 10. Cell lysates were immunoblotted as in A with PKR D-20. Numbers below are the proportion of PKR protein for each time point, normalized to actin and the mock PKR protein levels from the corresponding time point.

Figure 3.

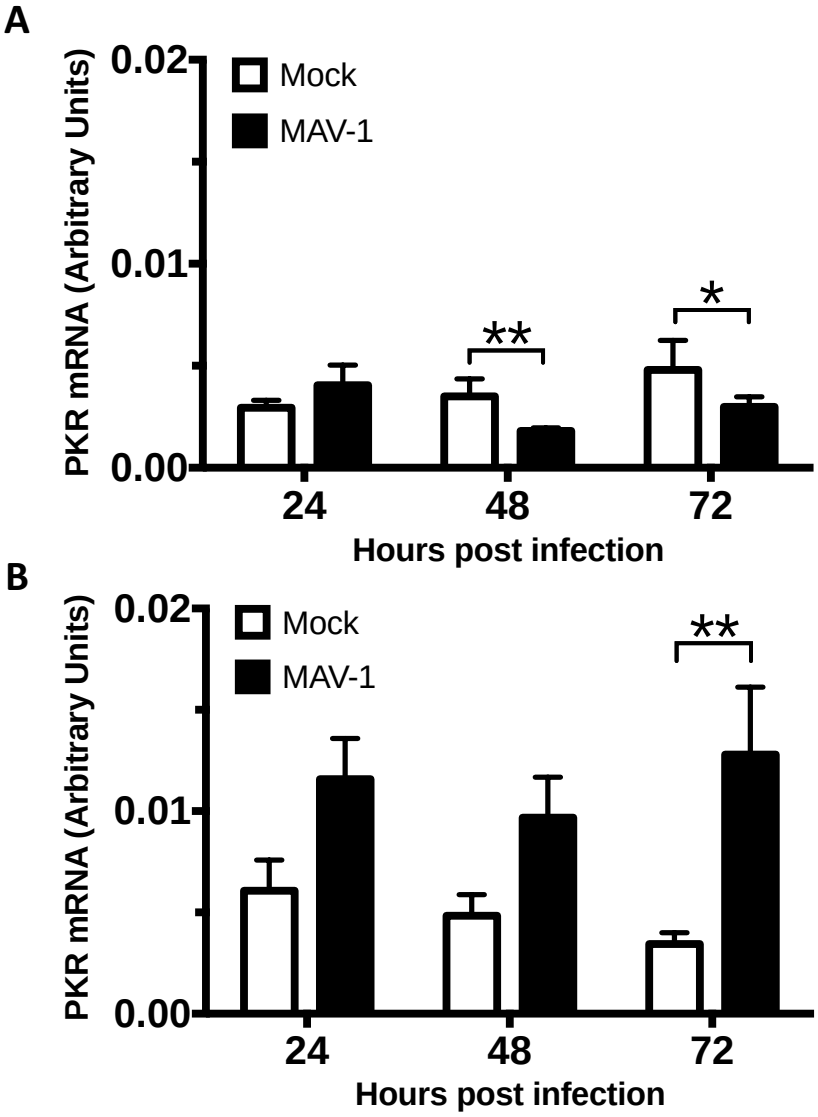

Figure 3. MAV-1 does not cause PKR depletion by reducing steady state levels of PKR mRNA at times when the protein levels are already reduced. MEFs (A) or isolated primary peritoneal macrophages (B) were harvested and infected with MAV-1 at an MOI of 10 or mock infected. The cell pellets were collected and RNA was isolated. cDNA was generated from the RNA, and qPCR was used to quantitate PKR mRNA levels. Each graph contains 5-7 replicates for each time point from three pooled experiments. Error bars show the SEM. *$P \leq 0.05$ and **$P \leq 0.01$.

Figure 4.

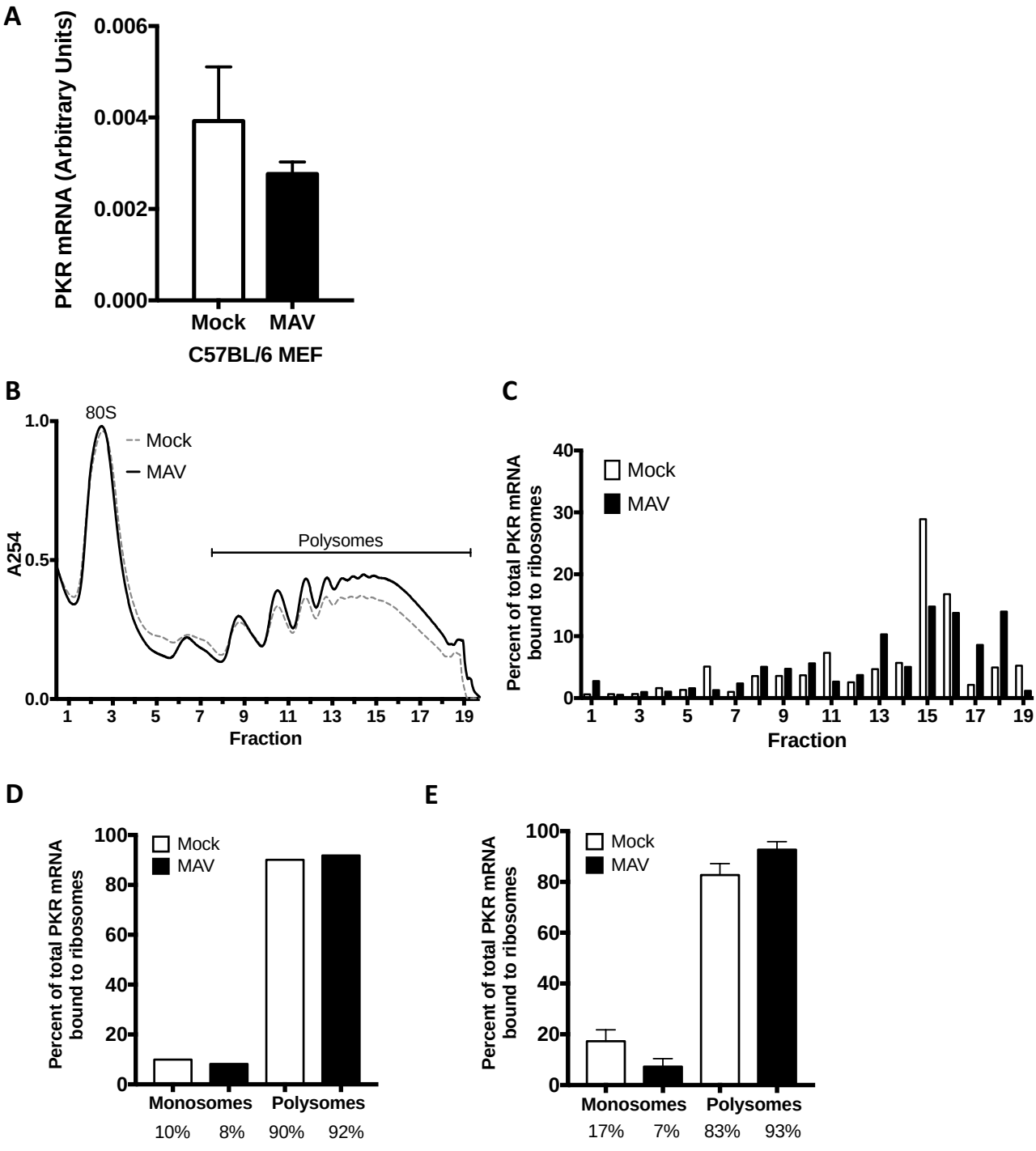

Figure 4. MAV-1 infection does not affect PKR translation. (A) C57BL/6 MEFs were infected with MAV-1 (MAV) at an MOI of 5 or mock infected (mock) and collected at 48 hpi. Cells were lysed, and cleared lysates from three 10 cm plates were layered onto 25% sucrose and centrifuged to pellet ribosomes. RNA was purified from the pellets, cDNA was generated from the RNA, and qPCR was used to quantitate the PKR mRNA levels. The graph contains 9 replicates for each time point, pooled from 3 independent experiments. Error bars show the SEM. (B) C57BL/6 MEFs were infected with MAV-1 (MAV) at an MOI of 2 or mock infected (mock). Cells were collected at 25 hpi and lysed; cleared lysates were layered onto 10-50% sucrose gradients and centrifuged. Gradients were collected from the top and pumped through a UV spectrophotometer, and 34 fractions were collected. The gradients are displayed with the bottom fractions to the right. The UV trace of the first 10 fractions (including 40S and 60S ribosomal subunits) is not shown. (C) RNA was purified from each fraction of the gradients in B. cDNA was generated from the RNA, and qPCR was used to quantitate PKR mRNA in each fraction and displayed as the percent of total PKR mRNA associated with ribosomes. B and C are results from one representative experiment of 3 independent experiments. (D) Percentage of total PKR mRNA associated with monosomes (fractions 1-6) and polysomes (fractions 7-19) from the trial displayed in B and C were pooled for mock and infected samples. The percentages represented by each bar are displayed below each bar. (E) Pooled monosome and polysome data as described in D from three independent experiments. Error bars show the SEM. The percentages represented by each bar are displayed below each bar. There were no significant differences between mock and infected samples (A, E).

Figure 5.

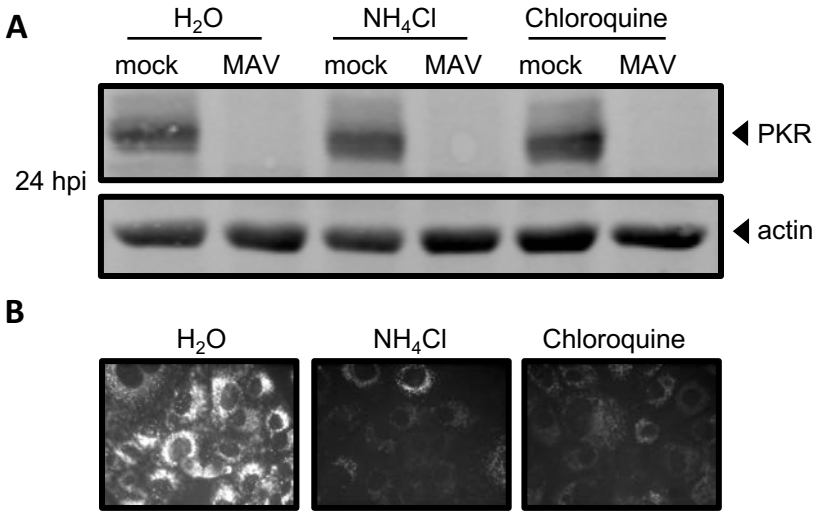

Figure 5. PKR is not depleted by lysosomal degradation during MAV-1 infection. (A) CMT93 cells were infected with MAV-1 (MAV) at an MOI of 10 or mock infected (mock) and treated with 10 mM ammonium chloride or 60 µM chloroquine to inhibit lysosomal degradation, or water, as a control. Cell lysates were analyzed by immunoblot with antibodies for PKR (D-20) and actin. Blots are representative of three independent experiments. (B) Inhibitors were tested for activity using a DQ BSA assay; the DQ BSA molecule will only fluoresce if lysosomal degradation is functional. Uninfected cells were treated as indicated and imaged by fluorescence microscopy.

Figure 6.

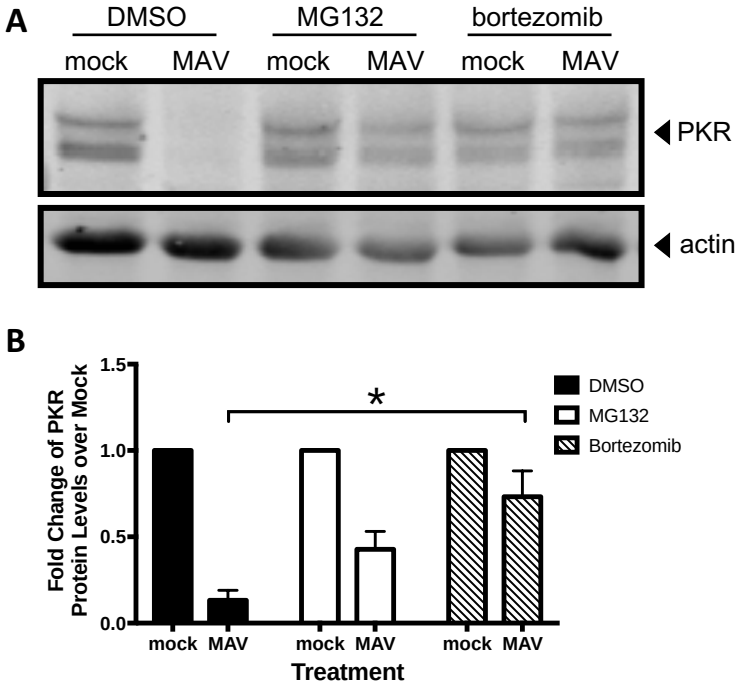

Figure 6. PKR is depleted by proteasomal degradation during MAV-1 infection. (A) C57BL/6 MEFs were infected with MAV-1 (MAV) at an MOI of 10 or mock infected (mock) and treated with DMSO (vehicle for inhibitors), 1 μM MG132, or 1 μM bortezomib. Cell lysates were were analyzed by immunoblot with antibodies for PKR (D-20) and actin. Blots are representative of four independent experiments. (B) Densitometry quantitation of four independent experiments. Treatment with bortezomib significantly inhibited PKR depletion in MAV-1 infected cells, $*P \leq 0.05$.

Figure 7.

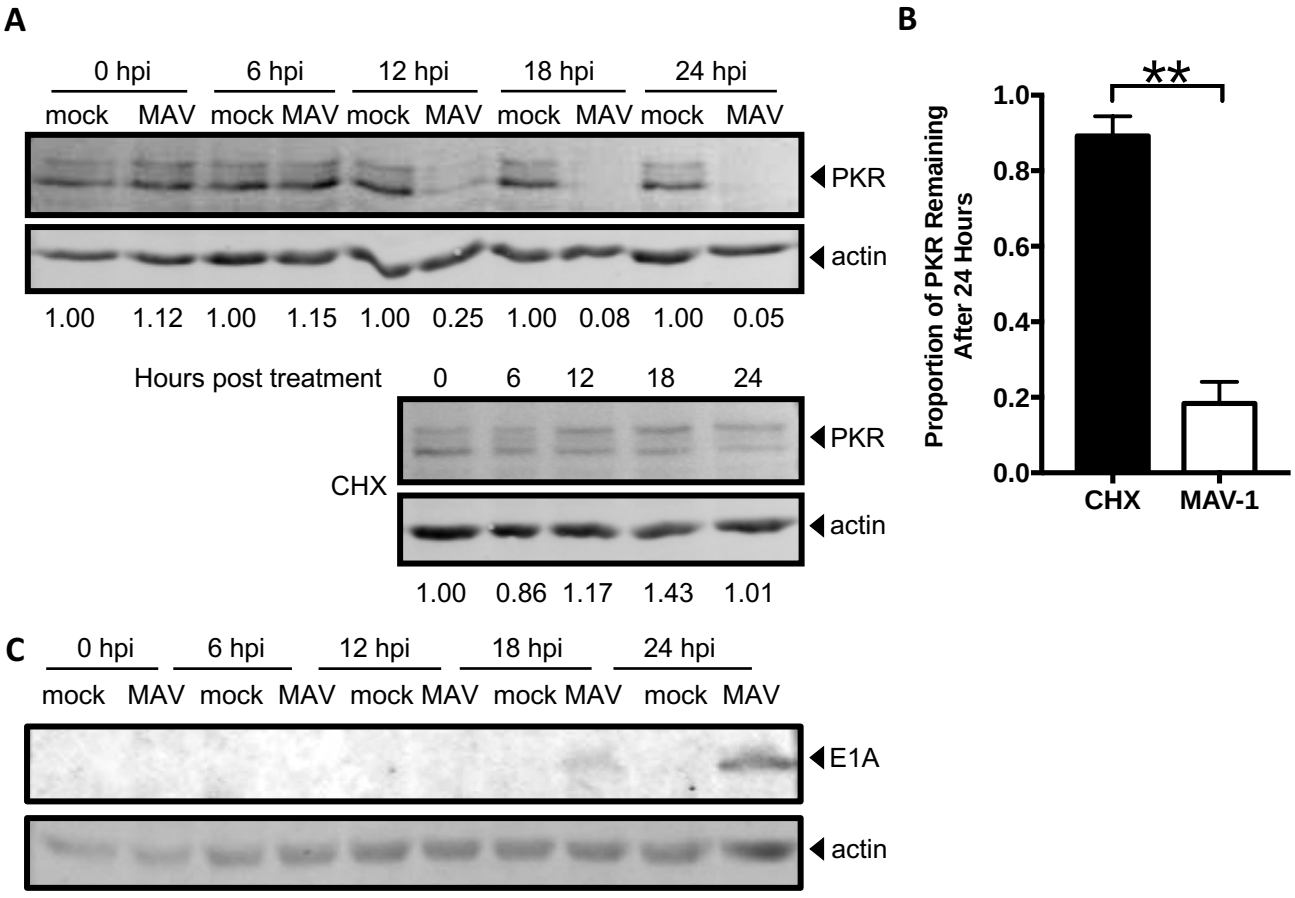

Figure 7. PKR is actively depleted early in infection. (A) CMT93 cells were infected with MAV-1 (MAV) at an MOI of 10 or mock infected (mock) (top), or uninfected cells were treated with 50 µg/mL cycloheximide (CHX, bottom) to inhibit elongation of protein synthesis. Cell lysates were analyzed by immunoblot with antibodies for PKR (D-20) and actin. Blots are representative of five independent experiments. (B) Densitometry quantitation of five independent experiments, $^{**}P \leq 0.01$. (C) CMT93 cell lysates from A were analyzed with a second immunoblot with antibodies for E1A and actin. Blots are representative of four replicates from two independent experiments. The E1A blot image was uniformly adjusted to a brightness of 30 and a contrast of 5 in Adobe Photoshop.

Figure 8.

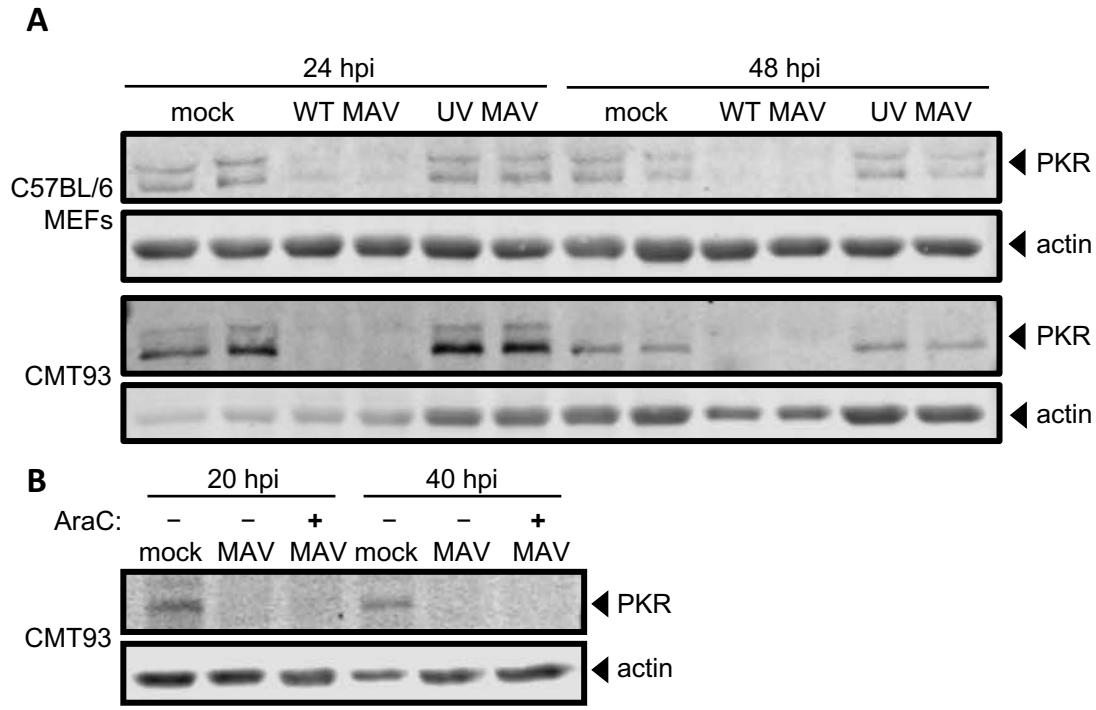

Figure 8. Early gene expression is required for PKR depletion by MAV-1. (A) Cells (as indicated at left) were infected with WT MAV-1 (WT MAV) or UV-inactivated MAV-1 (UV MAV) at an MOI of 10, or mock infected (mock). Cell lysates were analyzed by immunoblot with antibodies for PKR (D-20) and actin. Two independent wells were infected for each condition at both time points. (B) CMT93 cells were infected with WT MAV-1 (MAV) at an MOI of 10 or mock infected (mock). Infected cells were also treated (+) or not (-) with 20 µg/mL cytosine arabinasine (AraC), an inhibitor of DNA synthesis. Cell lysates were analyzed with antibodies for PKR and actin.

Supplemental Data Pieces

Supplemental Figure 1.

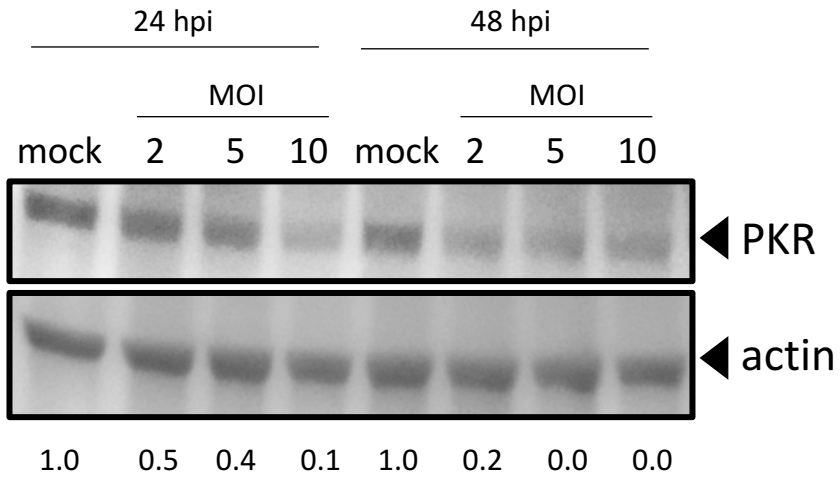

Supplemental Figure 1. PKR is depleted at MOIs of 2, 5, and 10. C57BL/6 MEFs were infected with MAV-1 at an MOI of 2, 5, or 10 (2, 5, 10) or mock infected (mock). Cell lysates were analyzed by immunoblot with antibodies for PKR (B-10) and actin. Densitometry quantitation using ImageJ is listed below each lane; for each time point, the infected samples were normalized to the mock. The PKR blot image was uniformly adjusted to a brightness of 150 in Adobe Photoshop.

Supplemental Figure 2.

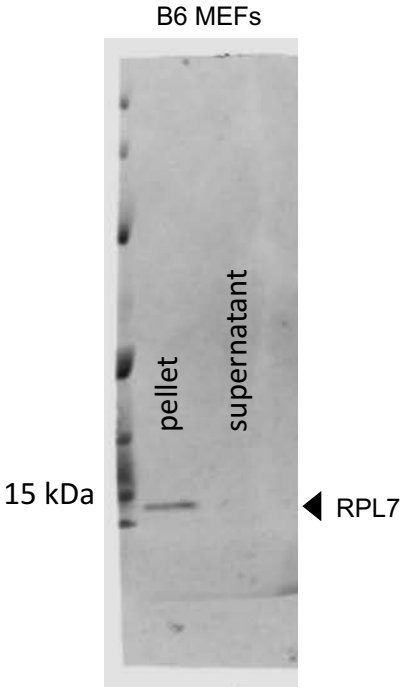

Supplemental Figure 2. Ribosome pelleting. To confirm that most ribosomes ended up in the pellet after centrifugation through sucrose (Fig. 4A), a sample of the pellet and the corresponding supernatant were analyzed by immunoblot with antibodies for RPL7 (ribosomal protein L7, Abcam, 1:2000, ab72550).

Supplemental Figure 3.

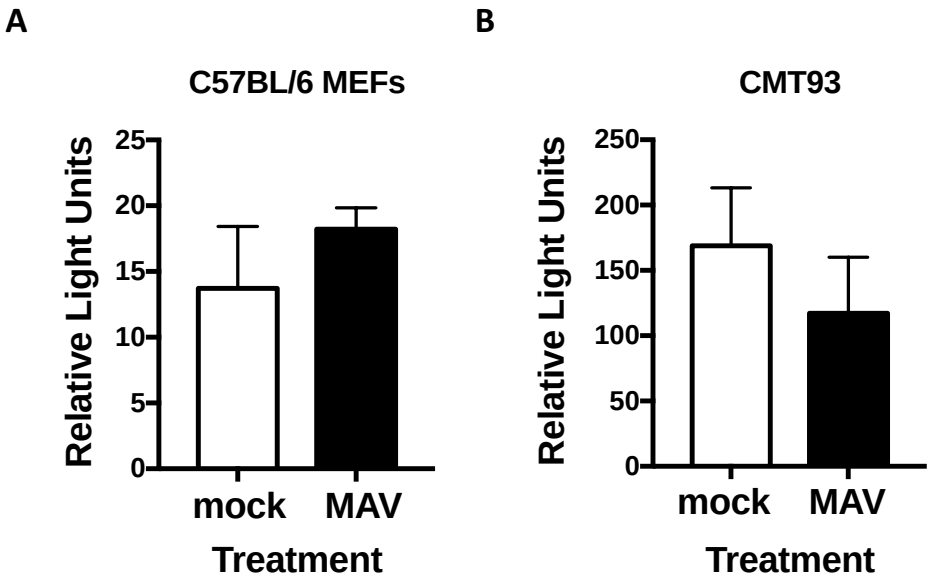

Supplemental Figure 3. PKR mRNA 5' UTR does not result in altered reporter protein levels upon MAV-1 infection. (A) C57BL/6 MEFs or (B) CMT93 cells were co-transfected with pmPKR5UTRfullNL or AUG-NL-3xFLAG and pGL4.13 using jetPRIME reagents (Polyplus #114-15) using the standard Polyplus protocol, with 200 ng total of plasmid and 300 µL of jetPRIME reagent per 35 mm well. At 24 hours after transfection, the cells were infected with MAV-1 at an MOI of 10. At 24 hpi, cells were lysed in 70 µL/well Glo Lysis Buffer (Promega Corp.). After lysing, 25 µL of each lysed sample and 25 µL of OneGlo or NanoGlo (Promega Corp.) was added to two wells in a black 96-well plate (Fisher Scientific #07-000-634). After 5 minutes, the plate was read on a Promega GloMax luminometer. Relative light units from the pmPKR5UTRfullNL plasmid were normalized to the firefly luciferase and positive control plasmids. Graphs are representative of 7-9 biological replicates per treatment group.

Supplemental Figure 4.

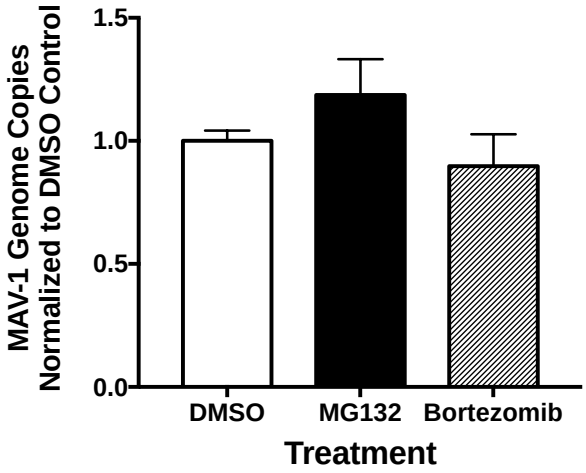

Supplemental Figure 4. MG132 and bortezomib treatment do not affect MAV-1 replication at 24 hpi. C57BL/6 MEFs were infected with MAV-1 at an MOI of 10 and treated with DMSO (vehicle for inhibitors), 1 μM MG132 or bortezomib, and collected at 24 hpi. DNA was purified from cell pellets and analyzed for MAV-1 genome copies by qPCR. Graph is representative of five biological replicates per treatment group. Error bars are standard error of the mean (SEM). $*P \leq 0.05$

Supplemental Figure 5.

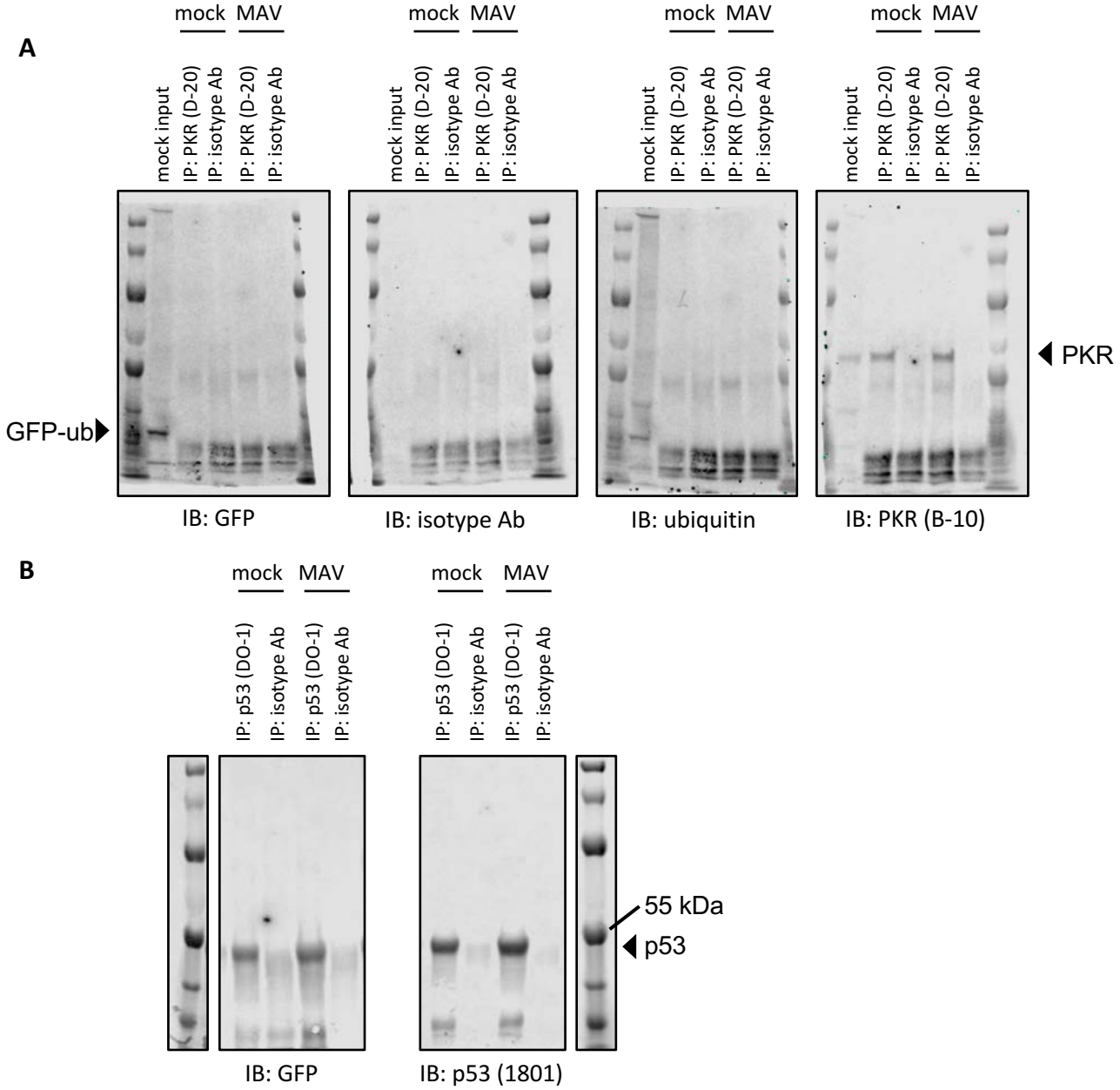

Supplemental Figure 5. PKR is not detectably ubiquitinated during MAV-1 infection. CMT93 cells were transfected with a GFP-ubiquitin plasmid using standard Polyplus transfection protocols. At 24 hpt, the cells were infected with MAV-1 (MAV) at an MOI of 5 or mock infected (mock) and treated with 10 μM MG132 at 6 hpi. Cell lysates were collected at 12 hpi and immunoprecipitated with (A) PKR (D-20) or an isotype control antibody or (B) p53 (DO-1) or an isotype control antibody. Immunoprecipitated samples were analyzed by immunoblot with GFP, ubiquitin, isotype, PKR (B-10), or p53 (1801) antibodies. Input lane (mock input) contains 0.008 volume of mock infected lysate (relative to volume in immunoprecipitations). For (B) GFP and p53 were probed on separate duplicate blots.

Supplemental Figure 6.

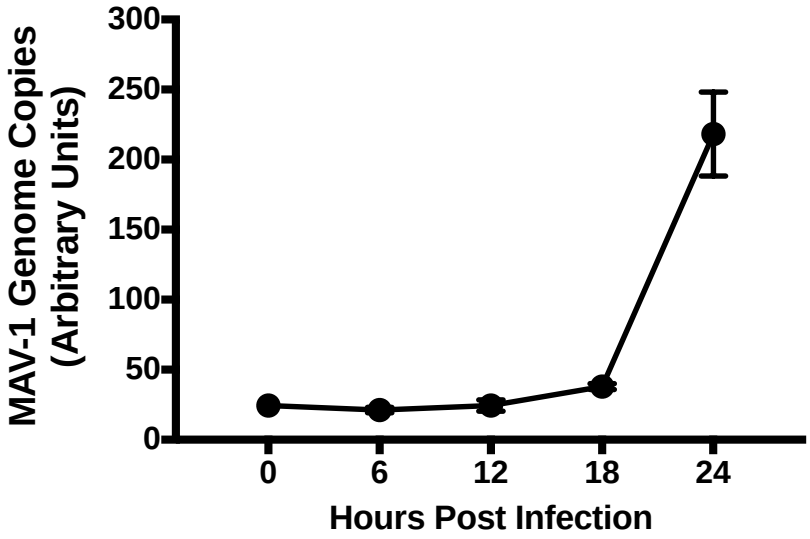

Supplemental Figure 6. Viral DNA replication can be detected at 24 hpi by qPCR. CMT93 cells were infected with MAV-1 (MAV) at an MOI of 10 and collected every 6 hours for 24 hours. DNA was purified from cell pellets and analyzed for MAV-1 genome copies by qPCR. Graph is representative of four to five biological replicates per treatment group. Error bars are standard error of the mean (SEM).

Supplemental Figure 7.

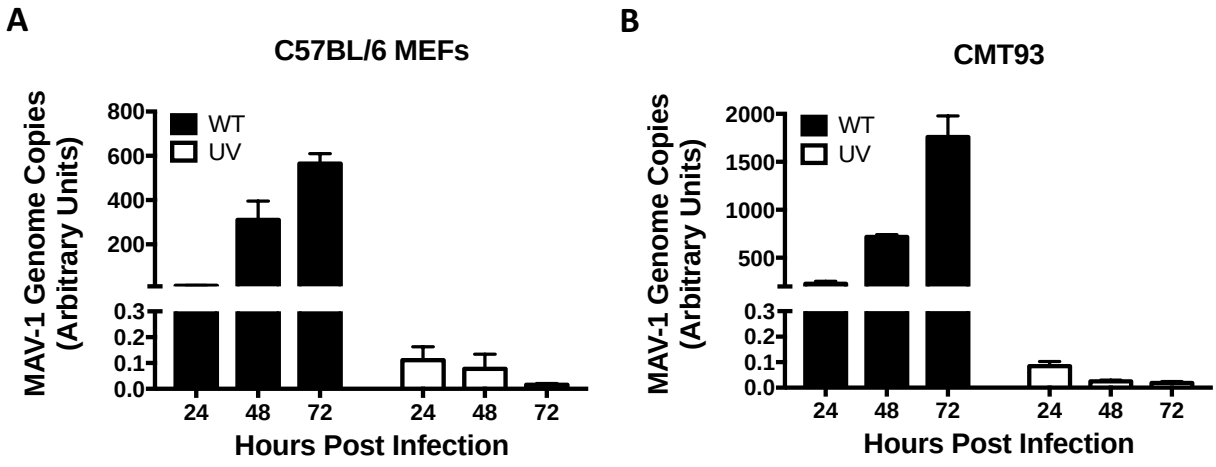

Supplemental Figure 7. UV-inactivated virus does not replicate viral DNA. (A) C57BL/6 MEFs or (B) CMT93 cells were infected with WT MAV-1 (WT) or UV-inactivated MAV-1 (UV) at an MOI of 10 and collected at indicated times. DNA was purified from cell pellets and analyzed for MAV-1 genome copies by qPCR. Graphs are representative of three to four biological replicates per treatment group. Error bars are standard error of the mean (SEM).

Supplemental Figure 8.

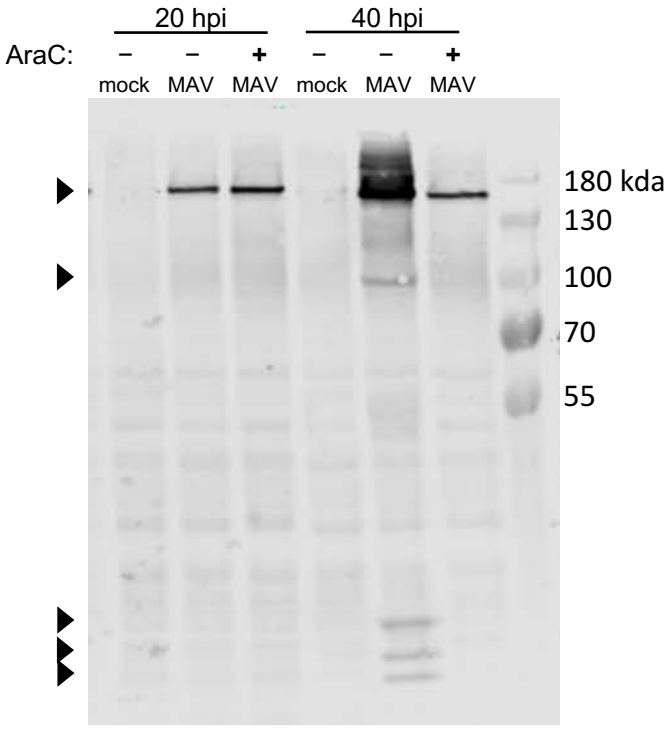

Supplemental Figure 8. AraC treatment inhibited late protein expression. CMT93 cells were infected with WT MAV-1 (MAV) at an MOI of 10 or mock infected (mock). Infected cells were also treated (+) or not (-) with 20 µg/mL cytosine arabinasine (araC), an inhibitor of DNA synthesis. Cell lysates were analyzed with antibodies for late virion proteins (AKO1-103, 1:1000). Arrowheads indicate late viral proteins.